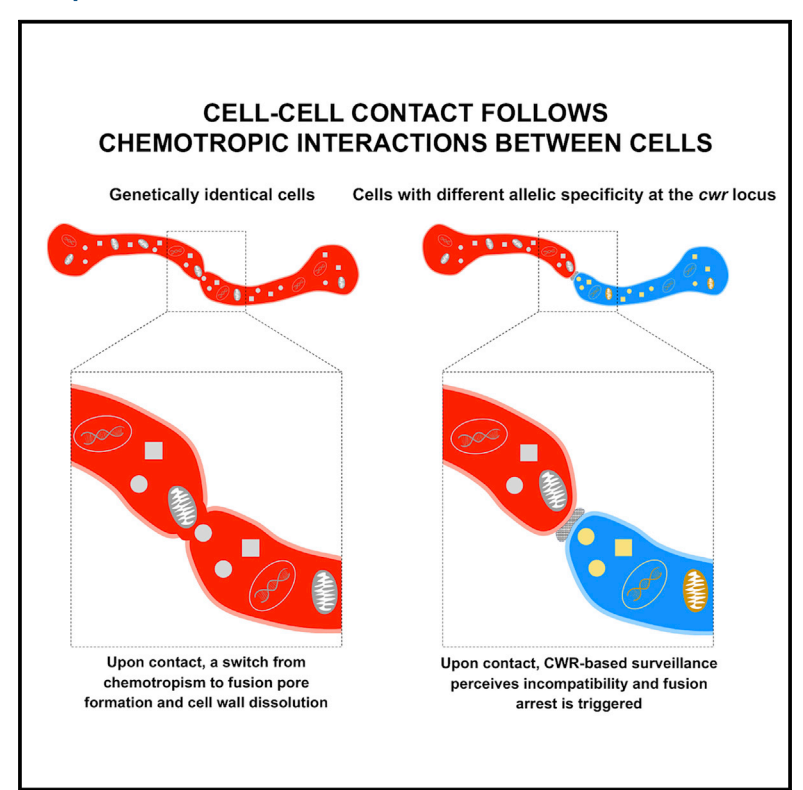
Current Biology

Allorecognition upon Fungal Cell-Cell Contact Determines Social Cooperation and Impacts the Acquisition of Multicellularity

Graphical Abstract



Authors

A. Pedro Gonçalves, Jens Heller, Elise A. Span, ..., Natalia Requena, Michael A. Marletta, N. Louise Glass

Correspondence

lglass@berkeley.edu

In Brief

Somatic cell fusion with conspecific partners entails risks of parasitism.

Gonçalves et al. present an allorecognition system, triggered upon cell-cell contact and leading to a blockage in cell wall dissolution, that prevents the formation of chimeras between genetically non-identical spores and hyphae of a model fungus.

Highlights

- Conspecific cooperation and cell fusion are crucial for microbial development
- Allorecognition upon contact blocks cell fusion of genetically non-identical cells
- Incompatible partners cannot switch from communication to cell wall dissolution mode
- The independent appearance of polymorphic cwr alleles suggests convergent evolution







Allorecognition upon Fungal Cell-Cell Contact Determines Social Cooperation and Impacts the Acquisition of Multicellularity

A. Pedro Gonçalves, ^{1,8,9} Jens Heller, ^{1,2,8} Elise A. Span, ^{3,10} Gabriel Rosenfield, ¹ Hung P. Do, ¹ Javier Palma-Guerrero, ^{1,11} Natalia Requena, ⁴ Michael A. Marletta, ^{5,6,7} and N. Louise Glass ^{1,2,12,*}

- ¹Department of Plant and Microbial Biology, University of California, Berkeley, Berkeley, CA 94720, USA
- ²Environmental Genomics and Systems Biology Division, Lawrence Berkeley National Laboratory, Berkeley, CA 94720, USA
- ³Biophysics Graduate Group, University of California, Berkeley, Berkeley, CA 94720, USA
- ⁴Molecular Phytopathology, Botanical Institute, Karlsruhe Institute of Technology, 76131 Karlsruhe, Germany
- ⁵Department of Chemistry, University of California, Berkeley, Berkeley, CA 94720, USA
- ⁶California Institute for Quantitative Biosciences, University of California, Berkeley, Berkeley, CA 94720, USA
- ⁷Department of Molecular and Cell Biology, University of California, Berkeley, Berkeley, CA 94720, USA
- ⁸These authors contributed equally
- ⁹Present address: Institute of Molecular Biology, Academia Sinica, Taipei 11529, Taiwan
- ¹⁰Present address: Zymergen, Emeryville, CA 94608, USA
- ¹¹Present address: Plant Pathology Group, Institute of Integrative Biology, ETH Zürich, 8092 Zürich, Switzerland
- 12Lead Contact
- *Correspondence: lglass@berkeley.edu https://doi.org/10.1016/j.cub.2019.07.060

SUMMARY

Somatic cell fusion and conspecific cooperation are crucial social traits for microbial unicellular-to-multicellular transitions, colony expansion, and substrate foraging but are also associated with risks of parasitism. We identified a cell wall remodeling (cwr) checkpoint that acts upon cell contact to assess genetic compatibility and regulate cell wall dissolution during somatic cell fusion in a wild population of the filamentous fungus Neurospora crassa. Nonallelic interactions between two linked loci, cwr-1 and cwr-2, were necessary and sufficient to block cell fusion: cwr-1 encodes a polysaccharide monooxygenase (PMO), a class of enzymes associated with extracellular degradative capacities, and cwr-2 encodes a predicted transmembrane protein. Mutations of sites in CWR-1 essential for PMO catalytic activity abolished the block in cell fusion between formerly incompatible strains. In Neurospora, alleles cwr-1 and cwr-2 were highly polymorphic, fell into distinct haplogroups, and showed trans-species polymorphisms. Distinct haplogroups and transspecies polymorphisms at cwr-1 and cwr-2 were also identified in the distantly related genus Fusarium, suggesting convergent evolution. Proteins in chemotropic processes extended localization at contact sites, suggesting that cwr regulates the transition between chemotropic growth and cell wall dissolution. Our work revealed an allorecognition surveillance system based on kind discrimination that inhibits cooperative

behavior in fungi by blocking cell fusion upon contact, contributing to fungal immunity by preventing formation of chimeras between genetically non-identical colonies.

INTRODUCTION

Complex multicellularity results from a developmental program that leads to differentiation of specialized structures and requires intercellular social cooperation [1]. In multicellular organisms, conspecific cooperation enhances adaptation to environmental variations due to the communal nature of produced goods (e.g., nutrients in a fungal colony). However, cooperation can cause conflict due to transmission of infectious elements and genotypes that negatively impact cellular fitness [2–6]. In this regard, high genetic relatedness and cooperation correlate positively to prevent exploitation of communal goods by cheaters [7–10].

The interconnected fungal mycelium is a prototype of a complex multicellular body. It operates as a polarized syncytium that expands via tip elongation and somatic cell-cell fusion [11, 12]. In *Neurospora crassa*, cell fusion between genetically identical cells (either germinated asexual spores [germlings] or between hyphae within a single colony) is a fitness character, as fusion mutants show a lag in colony development [3, 13]. Fusion between genetically non-identical cells results in a heterokaryotic syncytia that contains organelles of dissimilar genetic backgrounds. Although heterokaryon formation has been postulated to increase fitness in fungal populations [3], it is often precluded by allorecognition systems that either reduce somatic cell fusion between genetically distinct cells or cause cell death of fusion compartments [8, 14–16]. These allorecognition systems reduce transmission of mycoviruses, senescence plasmids, crippled

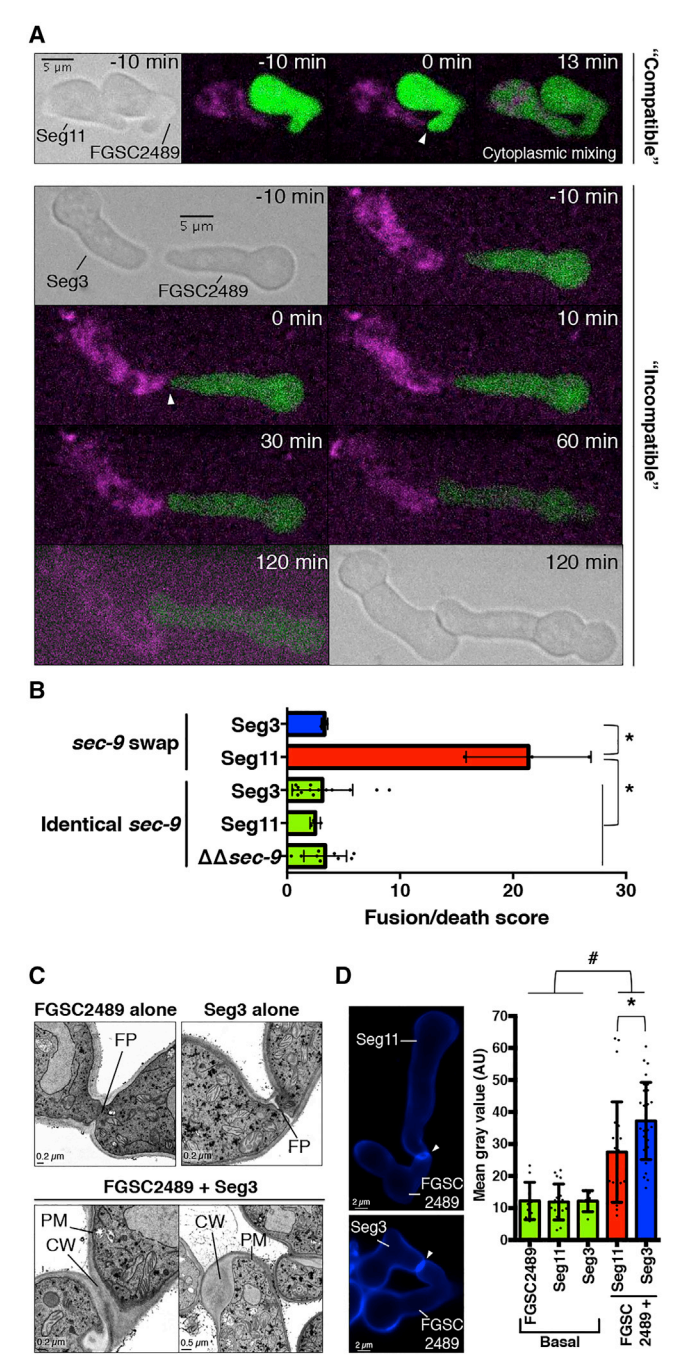


Figure 1. Cell-Wall-Associated Arrest Is Triggered to Prevent Cell **Fusion of Nonself Cells**

(A) GFP-expressing FGSC2489 germlings were paired with FM4-64-stained Seg11 (fusion-compatible, top) or Seg3 (fusion-incompatible, bottom) germlings, and cytoplasmic mixing (GFP exchange) was evaluated. Time point 0 was defined as the moment of cell-cell contact. Arrowheads indicate the zone of interaction between cells. See also Figure S1A and Videos S1 and S2. (B) Cell fusion as determined by propidium iodide (PI) uptake and flow cytometry. Indicated strains were paired with FGSC2489. Strains with identical sec-9 alleles: mixed cells show no cell death upon fusion (green). Strains with sec-9 swap alleles: mixed cells show cell death upon cell fusion (50% is theoretical maximum of cell death in this assay) [15]. *p < 0.0001 (one-way ANOVA followed by the Tukey post hoc test); $n \ge 3$. See also Figure S2.

mitochondria, and defective nuclei between fungal colonies [2-4, 6, 17].

To examine cooperation during the acquisition of multicellularity, we assessed fusion dynamics between wild Neurospora isolates that showed chemotropic interactions and identified a cell wall dissolution arrest phenotype following contact [11, 12]. A population genomics analysis led to identification of cell wall remodeling checkpoint loci (cwr-1 and cwr-2), whose allelic specificity regulates whether strains can transit from communication to cell wall dissolution and cell fusion. The cwr allorecognition checkpoint displays signs of balancing selection and convergent evolution in distinct fungal genera and allows cells to undergo kind recognition, presumably to avoid cooperation with disadvantageous partners during development of syncytial, multinucleate colonies.

RESULTS

A Cell Fusion Checkpoint Is Triggered upon Cell-Cell Contact

Previously, we reported that allelic specificity at determinant of communication (doc) loci determines pre-contact kind recognition in N. crassa by regulating chemotropic behavior prior to somatic cell fusion [16]. The wild-type strains, FGSC2489 and JW258, are unable to establish chemotropic interactions prior to somatic cell fusion because they belong to different doc haplogroups (CGH1 and CGH2, respectively). However, these two strains can mate and produce progeny able to communicate with only one of their parents [16]. We evaluated whether postchemotropic interactions were affected in progeny of the FGSC2489 × JW258 cross by staining germlings with FM4-64 and assessing cell fusion frequency when paired with an FGSC2489 strain expressing cytoplasmic GFP. Of these progeny, 62% underwent chemotropic interactions, cell fusion, and cytoplasmic mixing with FGSC2489 (Figure 1A, top; Video S1), and 38% did not show cell fusion and cytoplasmic mixing after chemotropic interactions and cell contact with FGSC2489 cells (Figure 1A, bottom; Video S2). Of progeny that underwent chemotropic interactions with JW258 cells, 52% showed cytoplasmic mixing with JW258, and 48% did not (Figure S1A). Over time, arrested cells redirected their growth, indicating that fusion was irreversibly blocked (Figure 1A, bottom).

To quantify cell fusion frequencies, we utilized a flow cytometry method based on a robust post-fusion death response mediated by genetic differences at sec-9 [15]. Isogenic germlings (identical sec-9 alleles) undergo cell fusion at high frequency and display low basal cell death levels (Figure 1B; Table S1), and germlings containing alternate sec-9 alleles (but otherwise isogenic) show similar fusion frequencies but high post-fusion

⁽C) Transmission electron microscopy of FGSC2489, Seg3, or FGSC2489 + Seg3 germling pairs, CW, cell wall; FP, fusion pore; PM, plasma membrane. (D) Mixtures of FGSC2489 cells with either Seq11 or Seq3 cells stained with calcofluor white. The mean gray value at the contact spot between cells (arrowheads) of ≥24 germlings pairs was quantified. "Basal" level of calcofluor white staining was obtained by quantifying cell wall segments in germlings not undergoing cell fusion (n \geq 6). *p = 0.0226; #p < 0.003 (one-way ANOVA followed by Tukey post hoc test).

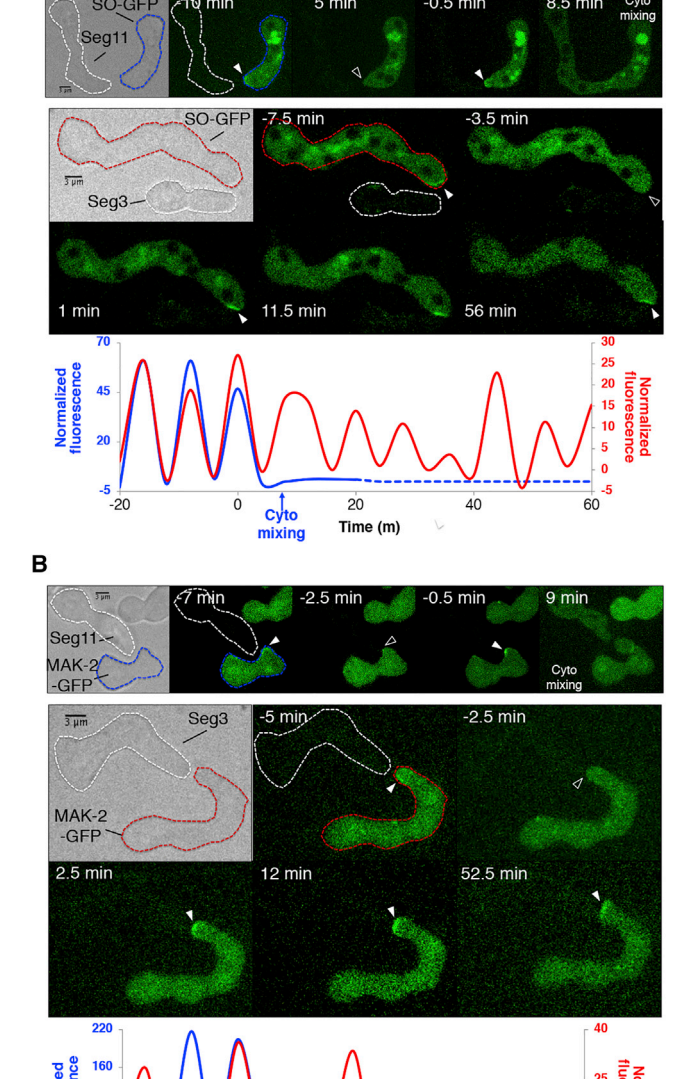


Figure 2. SOFT and MAK-2 Oscillations Continue at CAT Tips of Incompatible Fusion Partners after Contact

Time (m)

40

60

Ó

Cyto mixing

(A) FGSC2489 SOFT-GFP (SO-GFP) strain paired with Seg11 (compatible, top panels; blue line in plot) or Seg3 (incompatible, bottom panel; red line in plots); the mean fluorescence intensity at CAT tips was measured.

(B) FGSC2489 MAK-2-GFP strain paired with Seg11 (compatible, top panel; blue line in plot) or Seg3 (incompatible, bottom panel; red line in plots); the mean fluorescence intensity at CAT tips was measured.

Arrowheads indicate SOFT (A) or MAK-2 (B) localization at the zone of interaction; empty arrowheads indicate absence of SOFT (A) or MAK-2 (B) at CAT tips. Contact is defined as 0 min (time). Plots shown in (A) and (B) show oscillation of SOFT (A) or MAK-2 (B) to CAT tips over time with data from representative experiments. Arrows indicating "cyto mixing" in graphs indicates cytoplasmic mixing following cell fusion. Panels show representative experiments; $n \geq 4$.

See also Table S1.

-20

death rates [15]. Thus, introducing alternate sec-9 alleles in otherwise isogenic strains allowed us to use cell death as a proxy for fusion frequency. A program that allowed for automatic and unbiased gating and analysis of flow cytometry samples was generated (Figure S2). To assess cell fusion frequencies in progeny from the FGSC2489 × JW258 cross, we mixed FGSC2489 cells with Seg11 (progeny that undergoes chemotropic interactions and cell fusion with FGSC2489) or with Seg3 (progeny that undergoes chemotropic interactions but is blocked in cell fusion with FGSC2489). The relatively high death frequencies in FGSC2489 + Seg11 pairings and low death rates in FGSC2489 + Seg3 pairings indicated successful and blocked cell fusion, respectively (Figure 1B).

Transmission electron microscopy was used to assess whether cell fusion arrest observed for FGSC2489 + Seg3 pairings was due to failure in cell wall dissolution or in membrane merger. In samples of FGSC2489 cells alone or Seg3 cells alone, cell fusion was easily observed as indicated by dissolution of cell walls and plasma membrane at contact points (Figure 1C). In contrast, in mixtures of FGSC2489 + Seg3 cells, a high frequency of cell-cell contact sites showed an increase in cell wall material, consistent with a block in cell fusion during cell wall dissolution. To examine this phenotype further, we stained mixtures of FGSC2489 + Seg11 (compatible) versus FGSC2489 + Seg3 (incompatible) cells with the cell wall dye calcofluor white. Incompatible pairs of FGSC2489 + Seg3 germlings displayed significantly higher accumulation of dye at contact sites as compared to FGSC2489 + Seg11 pairs (Figure 1D). These data suggested that a cellular checkpoint is triggered upon cell-cell contact between genetically different cells that aborts fusion before cell wall dissolution is initiated.

Cell Fusion Arrest of Incompatible Cells Is Associatedwith Failure to Cease Communication

Members of a mitogen-activated protein kinase (MAPK) signaling complex (HAM-5/NRC-1/MEK-2/MAK-2) are recruited to fusion tips in germlings (termed conidial anastomosis tubes or CATs) [18] and to tips of fusion hyphae [12]. The MAK-2 complex assembles and disassembles at CAT tips every 8-10 min. A second protein complex bearing SOFT also assembles and disassembles at CAT tips but perfectly out of phase with the MAK-2 complex [19]. When FGSC2489 cells expressing either MAK-2-GFP or SOFT-GFP were paired with compatible Seg11 cells, MAK-2 and SOFT oscillated to CATs during chemotropic interactions and disappeared during cell wall dissolution and membrane merger (Figures 2A and 2B). In contrast, in arrested cell pairs (FGSC2489 + Seg3), MAK-2 and SOFT continued to oscillate at CAT tips long after cell contact (Figures 2A and 2B). These data indicated that germlings with a cell fusion block were unable to switch from communication to cell wall dissolution and membrane merger mode.

Cell Wall Remodeling Checkpoint Is Composed of Highly Polymorphic Linked Loci

To identify the causative locus of cell fusion arrest, we performed bulk segregant analysis (BSA) of progeny from the FGSC2489 \times JW258 cross. After whole-genome resequencing, a region spanning approximately 1 Mb on chromosome V was identified that showed 100% SNP segregation between



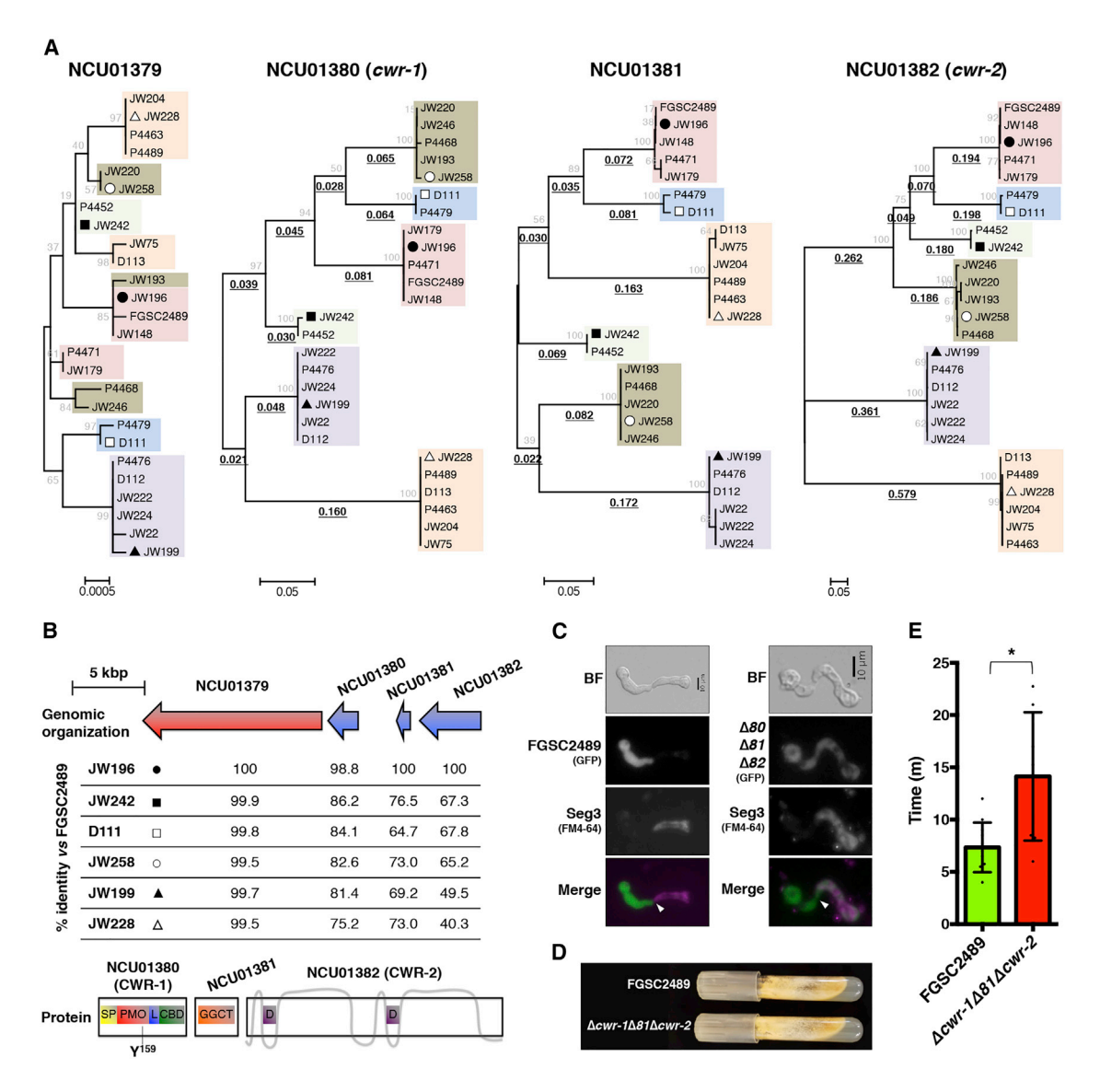


Figure 3. Identification of Genes Mediating Cell Fusion Arrest

(A) Amino acid sequences of NCU01379, NCU01380, NCU01381, and NCU01382 from 26 N. crassa isolates were used to build maximum-likelihood phylogenetic trees. Black underlined values below branches indicate length. Branch length values lower than 0.02 were omitted. Results from 100 bootstrap replicates are indicated at the nodes in gray. The six cwr haplogroups are indicated by rectangles of different colors. Selected isolates with correspondence to (B) are indicated with symbols. See also Figures S1B and S3.

(B) Graphical depiction of genomic organizations at the *cwr* region. The percentage of identity of the predicted protein sequences from wild isolates (JW196, JW242, D111, JW258, JW199, and JW228) was calculated using FGSC2489 as the reference. Conserved domains of NCU01380 (CWR-1), NCU01381, and NCU01382 (CWR-2) are shown. CBD, putative carbohydrate-binding domain; D, DUF3433 domain; GGCT, gamma-glutamylamine cyclotransferase domain; L, glycine- and serine-rich linker region; PMO, polysaccharide monooxygenase catalytic domain; SP, signal peptide. The predicted topology of CWR-2 transmembrane domains is shown in gray. See also Figure S4.

- (C) FM4-64-stained Seg3 cells were paired with FGSC2489 GFP strain (left, no fusion) or the triple mutant (ΔNCU01380ΔNCU01381ΔNCU01382) GFP strain (right, fusion). Arrowheads indicate the zone of interaction between cells.
- (D) Asexual development in slant tubes (7 days) for FGSC2489 and ΔNCU01380ΔNCU01381ΔNCU01382 strains.
- (E) Time to cytoplasmic mixing after cell contact was quantified in pairs of FGSC2489 germlings or ΔNCU01380ΔNCU01381ΔNCU01382 germlings (self-fusion pairings). *p = 0.0037 (Student's t test); n ≥ 8.

See also Tables S1 and S2.

FGSC2489 fusion-compatible and FGSC2489 fusion-incompatible pools of progeny DNA (Figure S1B). Using genomic sequences from 26 *N. crassa* isolates [15, 16, 20], we identified three linked genes (NCU01380, NCU01381, and NCU01382),

whose alleles showed high sequence diversity among individuals in this population and fell into six discrete haplogroups (Figure 3A). For example, the amino acid identity between FGSC2489 and JW228 for NCU01380, NCU01381, and

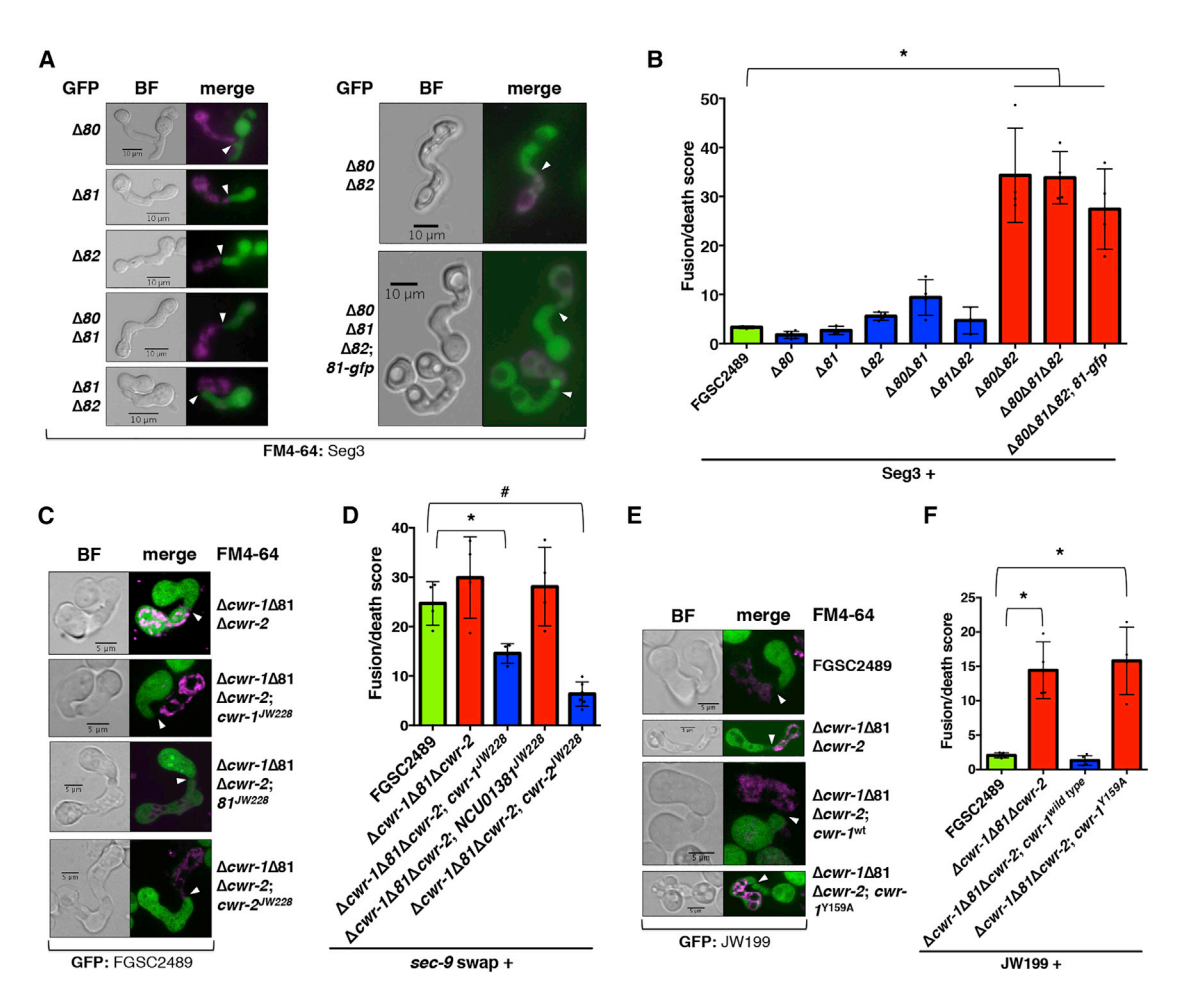


Figure 4. CWR-1 and CWR-2 Are Necessary and Sufficient to Induce Cell-Wall-Associated Arrest

(A) GFP-expressing cells (indicated on the left) were paired with FM4-64-stained Seg3 cells, and cytoplasmic mixing after cell contact (arrowhead) was evaluated. (B) Cell fusion as assayed by cell death score using sec-9 swap assay, as determined by PI uptake and flow cytometry, was measured for Seg3 cells paired with cells from indicated strains. *p < 0.0001 (one-way ANOVA followed by Tukey post hoc test); $n \ge 4$. Seg3 and indicated strains contained incompatible sec-9 alleles: cell death is a consequence of fusion of incompatible cells. with 50% the theoretical maximum. See also Figure S2.

- (C) FGSC2489-GFP cells were paired with indicated FM4-64-stained cells, and cytoplasmic mixing was evaluated upon contact (arrowheads).
- (D) Quantification of cell fusion as assayed by cell death was measured for pairings shown in (C). The FGSC2489 tester strain contained a sec-9 swap allele. *p < 0.001; #p < 0.0001 (one-way ANOVA followed by Tukey post hoc test); $n \ge 4$.
- (E) JW199-GFP cells were paired with indicated FM4-64-stained cells, and cytoplasmic mixing upon contact (arrowheads) was evaluated.
- (F) Cell fusion, as assayed by cell death, was measured for pairings assessed microscopically in (E). *p < 0.01 (one-way ANOVA followed by Tukey post hoc test); $n \ge 6$. Green, FGSC2489 control strain; blue, strains blocked in cell fusion; red, strains that undergo cell fusion. See also Tables S1 and S2.

NCU01382 was 75.2%, 73.0%, and 40.3%, respectively (Figure 3B). In contrast, NCU01379 showed 99.5% identity between FGSC2489 and JW228 (Figure 3B). The six haplogroups were completely conserved between alleles of NCU01380, NCU01381, and NCU01382 but only partially conserved for NCU01379 (Figure 3A), indicating recombination between NCU01379 and NCU01380-NCU01382.

The high sequence diversity observed for NCU01380, NCU01381, and NCU01382 is a property of genes involved in allorecognition, such as self-incompatibility loci in plants [21] and heterokaryon incompatibility loci in fungi [20, 22–24]. To test whether NCU01380, NCU01381, and/or NCU01382 were required for cell fusion arrest, we assessed the phenotype of mutants bearing deletions of NCU01380, NCU01381,

or NCU01382. Individual deletion strains Δ NCU01380, Δ NCU01381, and Δ NCU01382 were blocked in cell fusion with Seg3 cells (Figures 4A and 4B), a phenotype identical to parental strain FGSC2489. However, a strain bearing a deletion of all three genes (Δ NCU01380 Δ NCU01381 Δ NCU01382) underwent cell fusion with both FGSC2489 and Seg3 cells (Figures 3C and 4B).

To further test the hypothesis that allelic differences at NCU01380, NCU01381, and NCU01382 are causal for cell fusion arrest, we determined whether the block in cell fusion between wild isolates and FGSC2489 was dependent on NCU01380-NCU01382. First, we used strain JW196 (same haplogroup as FGSC2489; Figure 3A), and as predicted, JW196 fused with FGSC2489. However, cell fusion was blocked between



FGSC2489 and wild isolates from the other haplogroups (JW228, JW199, JW258, D111, and JW242; Figure S3). But when JW228, JW199, JW258, D111, or JW242 were paired with the triple-deletion strain ΔNCU01380ΔNCU01381ΔNCU01382, cell fusion was restored (Figure S3). These data confirmed that genetic differences at NCU01380, NCU01381, and NCU01382 were responsible for cell fusion arrest.

To determine whether all three genes were required for cell fusion arrest, we constructed double mutant strains ΔNCU01380 ΔNCU01381, ΔNCU01381 ΔNCU01382, and ΔNCU01380 ΔNCU01382. The double mutants ΔNCU01380 ΔNCU01381 and ΔNCU01381 ΔNCU01382 arrested during fusion in pairings with Seg3 cells. However, the ΔNCU01380 ΔNCU01382 double mutant underwent cell fusion with both FGSC2489 and Seg3 cells (Figures 4A and 4B). The triple mutant transformed with a GFP-tagged NCU01381 allele also underwent cell fusion with both FGSC2489 and Seg3 germlings (Figures 4A and 4B). These data indicated that allelic differences at NCU01380 and NCU01382, but not NCU01381, were required for the block in cell fusion. We named NCU01380 cell wall remodeling checkpoint-1 (cwr-1) and NCU01382 cell wall remodeling checkpoint-2 (cwr-2).

The morphological or growth phenotypes of any of the mutant combinations (including triple-deletion strain Δcwr-1ΔNCU01381Δcwr-2) were not significantly different from the parental FGSC2489 strain (Figure 3D). However, although triple mutant germlings underwent chemotropic interactions and self-fusion, they required significantly more time to fuse after contact, in comparison to FGSC2489 germlings (Figure 3E). These data indicated that cwr-1, NCU01381, and cwr-2 contributed to the efficiency of self-fusion events during cell wall dissolution.

To determine whether CWR-1 or CWR-2 were sufficient to induce cell fusion arrest, we cloned cwr-1, cwr-2, and NCU01381 alleles from JW228 (incompatible with FGSC2489; Figure S3). The cwr-1^{JW228}, cwr-2^{JW228}, and NCU01381^{JW228} alleles were transformed individually into the Δcwr -1ΔNCU01381Δcwr-2 mutant. Homokaryotic strains bearing cwr-1^{JW228}, cwr-2^{JW228}, or NCU01381^{JW228} alleles were paired with FGSC2489, and fusion frequency was assessed microscopically and by flow cytometry. Consistent with cwr-1 and cwr-2 playing an essential role in a cell wall remodeling checkpoint, expression of either cwr-1^{JW228} or cwr-2^{JW228} alleles in the triple deletion strain was sufficient to induce cell fusion arrest with an otherwise isogenic parental strain FGSC2489 (Figures 4C and 4D). These data also indicated that incompatibility functioned in trans (between cells), as a strain carrying only one allele at cwr-1 or cwr-2 was blocked in cell fusion with an incompatible strain.

cwr-1 Encodes a Polysaccharide Monooxygenase, and cwr-2 Encodes a Protein with Predicted **Transmembrane Domains**

cwr-1 encodes a predicted polysaccharide monooxygenase (PMO), with a signal peptide, a linker region rich in glycine and serine residues, and a carbohydrate-binding domain (Figure 3B). PMOs are an auxiliary activity (AA) within the carbohydrate-active enZYmes database [25]. CWR-1 shows substantial homology to a chitin-active copper-dependent AA11 PMO from Aspergillus oryzae [26] (Figure S4A). Of the 22 PMOs in N. crassa, four fell into the AA11 subtype, including NCU00822, NCU05932, NCU05404, and CWR-1 (Figure S4B). cwr-2 encodes a protein containing two DUF3433 (domain of unknown function) and eight predicted transmembrane regions (Figure 3B).

The PMO portion of CWR-1 contained conserved amino acid residues associated with catalytic activity, including the histidine brace and a hydrogen-bonding network (Figure S4A) [25]. To test whether PMO catalytic activity was essential for cell fusion arrest, an allele with a substitution of Y159A (cwr-1 Y159A) was constructed (Figures 4E and 4F). This tyrosine is strictly conserved among AA11 PMOs and, when mutated in other AA families, leads to loss in catalytic activity [27]. Although introduction of $\textit{cwr-1}^{\textit{FGSC2489}}$ into the triple-deletion mutant restored cell fusion arrest in pairings with incompatible JW199 cells, a triple-deletion mutant carrying cwr-1 Y159A underwent cell fusion. These data indicated that PMO catalytic activity is required for triggering the cell wall remodeling checkpoint.

Co-expression of Incompatible cwr-1 and cwr-2 Alleles within Single Cells Results in Asexual Developmental **Defects**

Our data indicated that cwr-1 or cwr-2 were sufficient for triggering cell fusion arrest in cells with incompatible cwr alleles. To investigate whether allelic versus non-allelic interactions were important for conferring this block, we expressed incompatible cwr-1/cwr-2 alleles in a single strain. The cwr-1^{JW228} and cwr-2JW228 alleles were introduced into FGSC2489 (i.e., containing cwr-1^{FGSC2489} cwr-2^{FGSC2489}); strains co-expressing incompatible cwr-1 and cwr-2 alleles produced shorter aerial hyphae and asexual spores that were paler than parental FGSC2489 spores (Figures 5A, 5B, and S5A). This phenotype was not observed when cwr-1JW228 and cwr-2JW228 alleles were co-expressed in the triple deletion mutant (Δcwr-1ΔNCU01381Δcwr-2; Figure S5A). Introduction of a cwr-1 allele from a different haplogroup (cwr-1^{D111}) into FGSC2489 also resulted in abnormal growth (Figures 5A and 5B). We used single-deletion strains of cwr-1 or cwr-2 (FGSC2489 background) expressing cwr-1^{JW228} or cwr-1^{D111} alleles to determine whether cwr-1 allelic interactions or cwr-1/cwr-2 non-allelic interactions were causative for the abnormal growth phenotype. Reversion from abnormal to wild-type morphology was observed when strains carried cwr-1^{JW228} or cwr-1^{D111} in a Δcwr-2 mutant background and in strains carrying cwr-2^{JW228} in a Δcwr-1 background (Figures 5A and 5B). These data indicated that non-allelic interactions between cwr-1 and cwr-2 were causal for the abnormal growth phenotype. FGSC2489; cwr-1^{JW228} asexual spores also displayed reduced germination, which was restored to wild-type levels when cwr-2 was deleted (Figure 5C).

From the phenotype of strains carrying incompatible cwr-1/ cwr-2 alleles, we predicted that these strains would also show a block in self-fusion. Indeed, despite undergoing chemotropic interactions, cytoplasmic mixing in self-pairings was not observed (Figures 5D and 5E). Consistent with cwr-1/cwr-2 non-allelic interactions being essential for this phenotype, the blocked self-fusion phenotype was reversed in cwr-1JW228 germlings carrying a Δcwr -2 deletion (Figures 5D and 5E).

Mutants that show defects in germling fusion almost always show a block in hyphal fusion [12, 19, 28]. To test whether hyphal

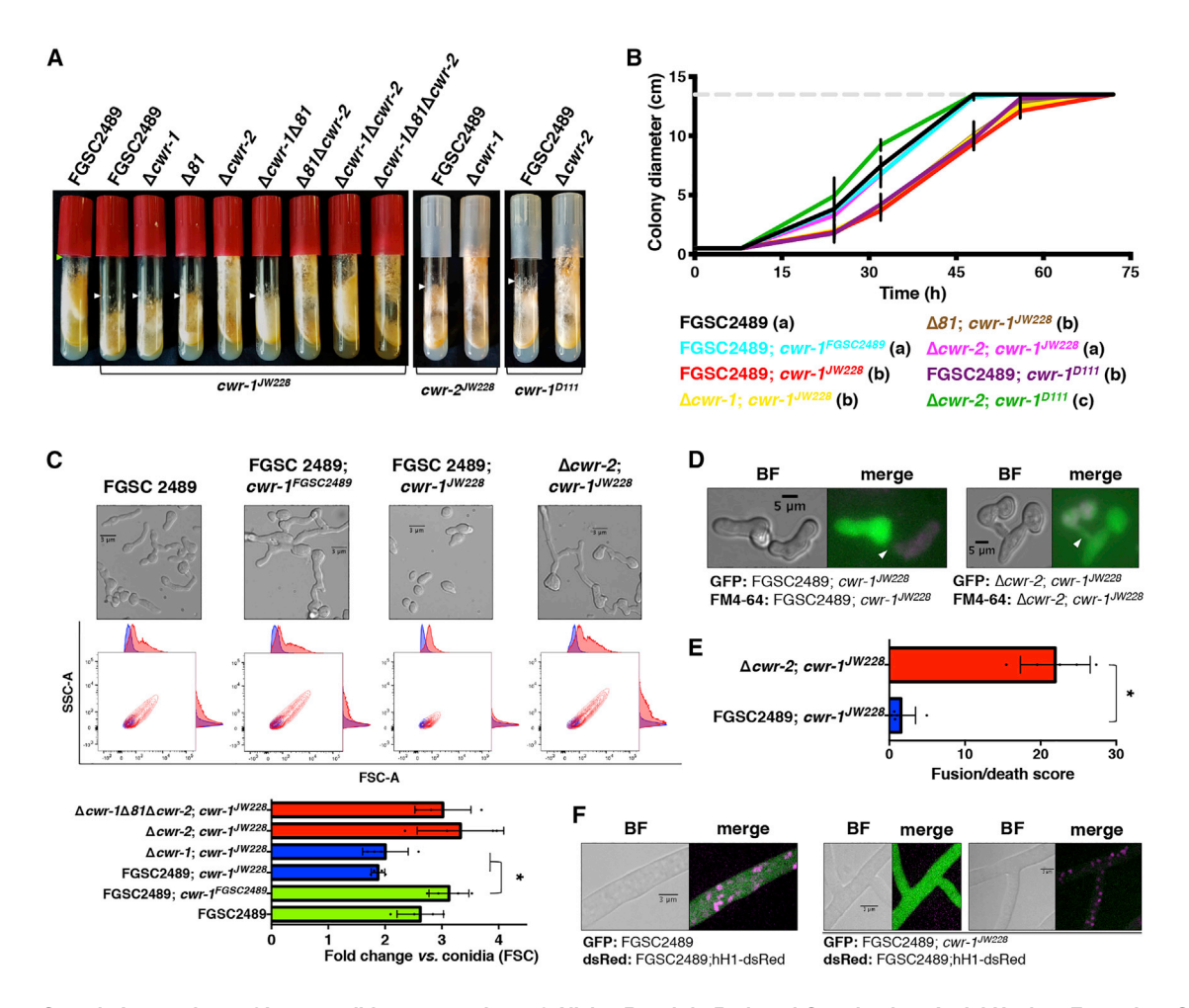


Figure 5. Genetic Interactions of Incompatible cwr-1 and cwr-2 Alleles Result in Reduced Germination, Aerial Hyphae Extension, Colony Establishment, and a Block in Cell Fusion

(A) Asexual development in slant tubes (7 days). Genes indicated below were introduced into the strain background indicated above. White arrowheads show aerial hyphae extension in comparison to FGSC2489 (green arrowhead). See also Figure S5.

- (B) Colony diameter after 72 h of growth with color key shown below. Permutation tests (5,000) were used to identify statistically significant differences (p < 0.05); samples within statistical groups are represented by lower case letters; $n \ge 4$. See also Figure S5B.
- (C) Bright-field micrographs (top panel) of 3.5-h-old germlings: strains co-expressing incompatible *cwr-1* and *cwr-2* alleles (third image) exhibit reduced germination. Middle panel shows flow cytometry contour plots of FSC (size) \times SSC (granularity) profiles of 4-h cultures (red) versus conidial samples (blue). Bottom panel shows fold change of the mean FSC of 4-h cultures relative to conidial samples. *p < 0.0314 (one-way ANOVA followed by Tukey post hoc test): n > 3.
- (D) Self-fusion in FGSC2489 cwr-1^{JW228} (left) or Δcwr-2 cwr-1^{JW228} (right) cells (isogenic cells expressing cytoplasmic GFP or FM4-64). Arrowheads indicate contact zone.
- (E) Cell fusion, as assayed by cell death, was determined by PI uptake and flow cytometry, of FGSC2489 $cwr-1^{JW228}$ or $\Delta cwr-2$ $cwr-1^{JW228}$ cells measured by pairing isogenic strains except for incompatible sec-9 alleles. *p < 0.0001 (Student's t test); n \geq 5. See also Figure S2.
- (F) Images of contact area between FGSC2489 hyphae expressing hH1-dsRed (FGSC2489 H1-dsRED) and either FGSC2489 (*cwr-1*^{FGSC2489})-GFP hyphae (left) or FGSC2489 (*cwr-1*^{JW228})-GFP (right) hyphae, which was visually inspected for hyphae co-expressing GFP and dsRED, indicating hyphal fusion has occurred. See also Tables S1 and S2.

fusion is blocked in *cwr*-incompatible cells, FGSC2489; *cwr*- 1^{JW228} cells expressing cytoplasmic GFP were co-inoculated 5 mm apart onto a plate with FGSC2489 cells expressing dsRED-H1 (a nuclear marker). Hyphae containing both cytoplasmic GFP and dsRED nuclei were not observed (Figure 5F), in contrast to fusion-compatible pairings between FGSC2489-GFP + FGSC2489-dsRED-H1 (Figure 5F). These data indicated that hyphal allorecognition was also regulated by allelic differences at the *cwr* loci.

CWR-1 and **CWR-2** Show Trans-species Polymorphisms and Convergent Evolution

Orthologs of CWR-1/CWR-2 were only found in the Pezizomycotina subphylum. In some species, *cwr-1* and *cwr-2* were linked, although outside of Sordariomycetes and Leotiomycetes, NCU01379 and NCU01381 were not linked to *cwr-1/cwr-2* (Figure S6A). To test whether allelic polymorphisms at CWR-1 and CWR-2 were retained in species where these loci are linked, we built phylogenetic trees that included multiple isolates of



N. tetrasperma, N. discreta, and various species of Fusarium (Table S3). In N. crassa and N. discreta, CWR-1 (Figure S6B) and CWR-2 (Figure 6) alleles clustered by haplogroup rather than by species, indicating that the age of allelic lines exceeds the age of speciation (7-10 mya) [29]. Six of the ten N. discreta isolates grouped into three N. crassa haplogroups, and the remaining four N. discreta isolates formed a haplogroup that was close to N. tetrasperma isolates (N. tetrasperma and N. crassa diverged 2.6-2.8 mya) [22]. In contrast, alleles of the highly conserved adjacent locus NCU01379 were reciprocally monophyletic (Figure 6). N. tetrasperma isolates did not show allelic differences at CWR-1 (Figure S6B) or CWR-2 (Figure 6), although they are polymorphic for other allorecognition loci [22, 30].

Alleles at the unlinked NCU01381 locus grouped by Fusarium species (Figure S6B), and, similar to N. crassa, linked cwr-1 (Figure S6B) and cwr-2 (Figure 6) loci showed allelic lineages. For example, ten orthologs of cwr-1/cwr-2 from F. fujikuroi fell into four haplogroups, and four F. verticillioides sequences fell into three haplogroups, with two of three haplogroups in F. verticillioides clustering with three haplogroups of F. fujikuroi. Thus, in both Neurospora and Fusarium, cwr-1/ cwr-2 alleles showed trans-species polymorphisms, which is typical of allorecognition genes [20, 22, 23]. However, cwr-1/ cwr-2 haplogroups did not extend beyond genera (Figures 6 and S6B), indicating convergent evolution. This conclusion was supported by the lack of cwr-1/cwr-2 allelic haplogroups in N. tetrasperma, suggesting that polymorphisms at these loci can be repeatedly lost and gained.

We calculated the average evolutionary diversity of cwr-1/ cwr-2 alleles in Neurospora and Fusarium, in isolates of Trichoderma harzianum, and in the plant pathogen Zymoseptoria tritici, with NCU01379 orthologs as an example of a non-diverse locus. cwr-1/cwr-2 alleles showed increased diversity in all species except N. tetrasperma (Figure S6C), and diversity of cwr-linked NCU01381 alleles was only increased in N. crassa and N. discreta (Figure S6C).

DISCUSSION

In this study, we showed that cooperative cell fusion is under surveillance of an allorecognition checkpoint triggered by cell-cell contact. This checkpoint is controlled by two linked loci (cwr-1 and cwr-2) with highly polymorphic alleles that segregated into discrete haplogroups. These two loci showed strict linkage disequilibrium and trans-species polymorphisms, consistent with balancing selection acting at these loci. N. crassa cells that harbored incompatible cwr alleles failed to initiate cell wall dissolution at the zone of contact and displayed extended MAK-2 and SOFT signaling, indicating an inability to transit between chemotropism and cell wall dissolution. CWR allorecognition acts in a negative manner, as cells containing alternate cwr alleles were blocked in cell fusion, and a strain carrying deletions of cwr-1 and cwr-2 underwent fusion with formerly incompatible cells. The cwr-1 and cwr-2 loci were not essential for self-fusion, although the Δcwr-1ΔNCU01381 Δcwr-2 mutant showed a slight delay in cell fusion, indicating that the CWR system is not necessary for fusion between compatible cells but rather blocks fusion between incompatible partners. The identification of CWR checkpoint in N. crassa will enable investigations into how the transition from adhesion to cell wall dissolution occurs, a process that is not well understood in fungi.

In the N. crassa genome, but not in other fungi, cwr-1 and cwr-2 are separated by NCU01381, which was dispensable for cell fusion arrest in N. crassa. Allelic diversity at NCU01381 is likely due to genetic hitchhiking, as NCU01381 was not identified in the cwr-1/cwr-2 cluster in other species. Syntenic cwr-1/ cwr-2 pairs were only found in species in the Pezizomycotina, supporting the role of CWR proteins in cooperation and acquisition of complex multicellularity, which arose in this lineage 443-695 mya [31]. The linkage of cwr-1/cwr-2 and TSP in Fusarium suggests that these loci could also regulate allorecognition in other fungi; Fusarium species are able to undergo germling CAT and hyphal fusion [32]. However, the fact that cwr-1/cwr-2 haplotypes have not been maintained between Neurospora and Fusarium suggests repeated recruitment of these loci for allorecognition. This hypothesis is consistent with observations for sec-9/plp-1-mediated allorecognition; these two polymorphic loci regulate allorecognition in N. crassa, Podospora anserine, and Cryphonectria parasitica [15, 33], but polymorphisms segregate by genus rather than haplogroup [15].

Non-allelic interactions between cwr-1 and cwr-2 were necessary and sufficient to activate allorecognition and block cell fusion. CWR-1 is predicted to be a PMO11, and a mutation predicted to ablate catalytic activity abolished allorecognition. PMOs are typically active on recalcitrant polysaccharides [25], and the only characterized PMO11 acts on chitin [26], a fungal cell wall component. In one model for allorecognition, a specific cell wall modification by CWR-1 from a particular haplogroup would generate a signaling product, perhaps chitin-derived, that interacts with CWR-2; CWR-2 is a predicted transmembrane protein and could function as a receptor. However, this hypothesis would require CWR-1 from each haplogroup to form an allele-specific cell wall modification, which is not consistent with current models of PMO function [25]. An alternative model predicts interactions between non-cognate CWR-1 and CWR-2 proteins, where a conformational change in CWR-1 resulting from its catalytic activity leads to recognition by a non-cognate CWR-2. In this model, predicted catalytically inactive versions of CWR-1 (CWR-1 Y159A) would be incapable of polysaccharide degradation and presentation to its non-cognate CWR-2, allowing fusion to proceed. Further experiments to define regions of allelic specificity of CWR-1 and CWR-2, protein-protein interactions, biochemical analyses of CWR-1 from different haplogroups, and genetic suppression analyses will expand our knowledge on the molecular basis of allorecognition and cell fusion regulation by the CWR system.

By harnessing the power of population genomics, we identified three allorecognition checkpoints that act at distinct levels during early stages of cooperation and acquisition of multicellularity in filamentous fungi. The first checkpoint is regulated by allelic specificity at doc loci, where non-identity negatively regulates chemotropic interactions by preventing reinforcement of MAPK signaling [16]. The second checkpoint assesses identity at cwr loci and negative regulates the transition from cell adhesion to cell wall dissolution. Cell fusion can occur if cells have identical doc and cwr loci, but a third post-fusion checkpoint can trigger germling-regulated death. Allorecognition in this case is mediated by allelic differences at two linked loci, sec-9

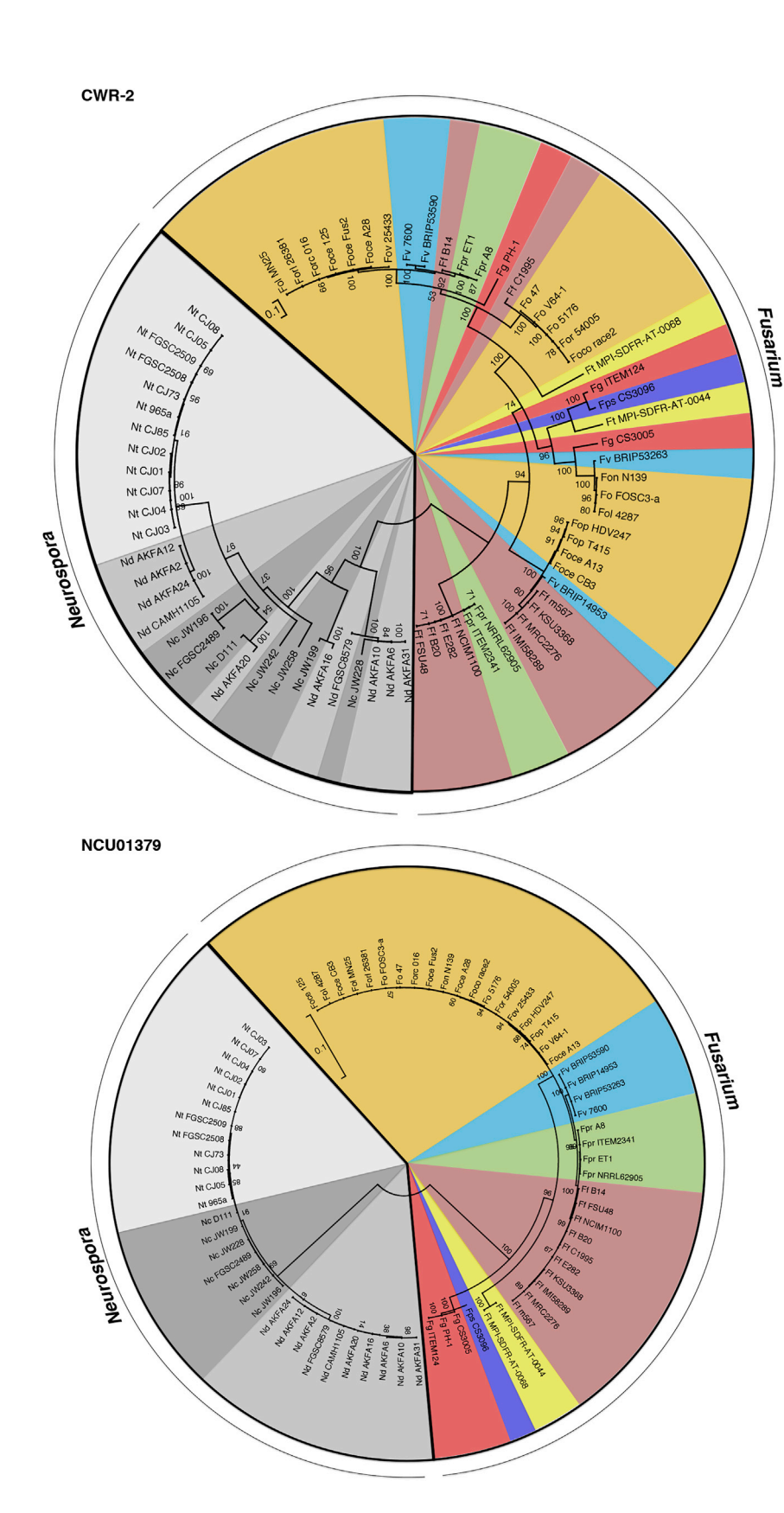


Figure 6. CWR Orthologs Show Features of **Balancing Selection and Convergent Evolu**tion

Amino acid sequences of CWR-2 and NCU01379 from indicated isolates were used to build maximum-likelihood phylogenetic trees. Results from 100 bootstrap replicates are indicated in gray. Strains of the same species are shaded with identical colors; light gray, N. tetrasperma; medium gray, N. discreta; dark gray, N. crassa; light yellow, F. tricinctum; yellow, F. oxysporum; pink, F. fujikuroi; red, F. graminearum; green, F. proliferatum; blue, F. verticillioides; purple, F. pseudograminearum. See also Figure S6. Phylogenetic trees of CWR-1 and NCU01381 are shown in Figure S6B. Abbreviations and accession numbers are described in Table S3.



and plp-1, which encode a SNARE and a fungal nucleotide oligomerization domain (NOD)-like receptor, respectively [15]. Unlike the doc, cwr, and sec-9/plp-1 loci, which function in allorecognition in germlings and hyphae, genetic differences at het loci regulate heterokaryon formation following hyphal fusion; if hyphae differ in allelic specificity at a het locus, fusion compartments are walled off and rapidly killed [14, 34]. The existence of multiple allorecognition checkpoints prior and post cell fusion in N. crassa suggests an evolutionary pressure to avoid somatic nonself cooperation at all costs. Indeed, considering haplogroups identified for doc [16], cwr, sec-9/ plp-1 [15], and 12 het loci in N. crassa [20, 22], the likelihood of productive cell fusion events between non-identical cells is extremely small (~1,105,920 possible incompatible genotypes). Importantly, mechanisms regulating somatic allorecognition are suppressed during sexual reproduction, as wild isolates with allelic specificity differences at doc, cwr, sec-9/plp-1, and het loci are able to productively mate and produce meiotic progeny.

Examples of allorecognition upon cell-cell contact have been documented in the protochordate Botryllus schlosseri, where an inflammatory response resulting in allograft rejection is triggered upon contact between two colonies that lack identity at fuhc [35]. In the social amoeba Dictyostelium discoideum, kin discrimination is mediated by direct binding of adhesion proteins TgrB1 and TgrC1 [10, 36]. In fungi, social cooperation and cell fusion enables interconnectedness of the mycelium, a network where public goods like organelles or nutrients are shared and transported over long distances [11, 12, 37, 38]. The mycelial soma is vulnerable to mycoparasites and/or cheaters that can gain access to the community via cell fusion, potentially exploiting shared resources and disturbing multicellular development [7, 8]. Hence, syncytial organisms, such as filamentous fungi, rely on allorecognition to ensure clonality, reducing the risk of transfer of infectious agents and cheaters and permitting formation of a fit cellular network consisting of near isogenic individuals with optimized competency to expand, forage, and mate.

STAR*METHODS

Detailed methods are provided in the online version of this paper and include the following:

- KEY RESOURCES TABLE
- LEAD CONTACT AND MATERIALS AVAILABILITY
- EXPERIMENTAL MODEL AND SUBJECT DETAILS
 - Neurospora crassa
- METHOD DETAILS
 - O PCR
 - Transformation
 - Epifluorescence and confocal microscopy
 - Flow cytometry
 - Transmission electron microscopy
 - Radial growth
 - O Bulk segregant analysis (BSA)
 - Bioinformatics
- QUANTIFICATION AND STATISTICAL ANALYSIS
- DATA AND CODE AVAILABILITY

SUPPLEMENTAL INFORMATION

Supplemental Information can be found online at https://doi.org/10.1016/j. cub.2019.07.060.

ACKNOWLEDGMENTS

We thank Marcus Roper (UC-Los Angeles) for his assistance with flow cytometry analyses. This work was supported in part by a National Science Foundation grant (MCB1412411) and a Laboratory Directed Research and Development Program of Lawrence Berkeley National Laboratory under US Department of Energy contract no. DE-AC02-05CH11231 to N.L.G. We thank the Berkeley Flow Cytometry Facility, the Robert D. Ogg Electron Microscope Laboratory, and the CNR Biological Imaging Facility for their technical support. This work used the Vincent J. Coates Genomics Sequencing Laboratory (UC Berkeley), supported by NIH S10 Instrumentation Grants S10RR029668 and S10RR027303.

AUTHOR CONTRIBUTIONS

A.P.G., J.H., M.A.M., and N.L.G. designed the study and experiments. A.P.G. and N.L.G. wrote the article. E.A.S. performed strain construction and analyzed the PMO family distribution. G.R. generated the flow cytometry analysis software. H.P.D. performed the calcofluor white-based cell wall measurements. J.P.-G. assisted in the bulk segregant analysis. N.R. contributed to the phylogenetic analysis.

DECLARATION OF INTERESTS

The authors declare no competing interests.

Received: June 2, 2019 Revised: July 16, 2019 Accepted: July 19, 2019 Published: August 29, 2019

REFERENCES

- 1. Knoll, A.H. (2011). The multiple origins of complex multicellularity. Annu. Rev. Earth Planet. Sci. 39, 217-239.
- 2. Bastiaans, E., Aanen, D.K., Debets, A.J., Hoekstra, R.F., Lestrade, B., and Maas, M.F. (2014). Regular bottlenecks and restrictions to somatic fusion prevent the accumulation of mitochondrial defects in Neurospora. Philos. Trans. R. Soc. Lond. B Biol. Sci. 369, 20130448.
- 3. Bastiaans, E., Debets, A.J., and Aanen, D.K. (2015). Experimental demonstration of the benefits of somatic fusion and the consequences for allorecognition. Evolution 69, 1091-1099.
- 4. Biella, S., Smith, M.L., Aist, J.R., Cortesi, P., and Milgroom, M.G. (2002). Programmed cell death correlates with virus transmission in a filamentous fungus. Proc. Biol. Sci. 269, 2269-2276.
- 5. Fernàndez-Busquets, X., Körnig, A., Bucior, I., Burger, M.M., and Anselmetti, D. (2009). Self-recognition and Ca2+-dependent carbohydrate-carbohydrate cell adhesion provide clues to the cambrian explosion. Mol. Biol. Evol. 26, 2551-2561.
- 6. Zhang, D.X., Spiering, M.J., Dawe, A.L., and Nuss, D.L. (2014). Vegetative incompatibility loci with dedicated roles in allorecognition restrict mycovirus transmission in chestnut blight fungus. Genetics 197, 701-714.
- 7. Aanen, D.K., Debets, A.J., de Visser, J.A., and Hoekstra, R.F. (2008). The social evolution of somatic fusion. BioEssays 30, 1193-1203.
- 8. Bastiaans, E., Debets, A.J., and Aanen, D.K. (2016). Experimental evolution reveals that high relatedness protects multicellular cooperation from cheaters. Nat. Commun. 7, 11435.
- 9. Diggle, S.P., Griffin, A.S., Campbell, G.S., and West, S.A. (2007). Cooperation and conflict in quorum-sensing bacterial populations. Nature 450, 411-414.

- Kuzdzal-Fick, J.J., Fox, S.A., Strassmann, J.E., and Queller, D.C. (2011).
 High relatedness is necessary and sufficient to maintain multicellularity in *Dictyostelium*. Science 334, 1548–1551.
- Glass, N.L., Rasmussen, C., Roca, M.G., and Read, N.D. (2004). Hyphal homing, fusion and mycelial interconnectedness. Trends Microbiol. 12, 135–141.
- Fischer, M.S., and Glass, N.L. (2019). Communicate and fuse: how filamentous fungi establish and maintain an interconnected mycelial network. Front. Microbiol. 10, 619.
- Richard, F., Glass, N.L., and Pringle, A. (2012). Cooperation among germinating spores facilitates the growth of the fungus, *Neurospora crassa*. Biol. Lett. 8, 419–422.
- Gonçalves, A.P., Heller, J., Daskalov, A., Videira, A., and Glass, N.L. (2017). Regulated forms of cell death in fungi. Front. Microbiol. 8, 1837.
- Heller, J., Clavé, C., Gladieux, P., Saupe, S.J., and Glass, N.L. (2018). NLR surveillance of essential SEC-9 SNARE proteins induces programmed cell death upon allorecognition in filamentous fungi. Proc. Natl. Acad. Sci. USA 115, E2292–E2301.
- Heller, J., Zhao, J., Rosenfield, G., Kowbel, D.J., Gladieux, P., and Glass, N.L. (2016). Characterization of greenbeard genes involved in long-distance kind discrimination in a microbial eukaryote. PLoS Biol. 14, e1002431.
- Debets, F., Yang, X., and Griffiths, A.J. (1994). Vegetative incompatibility in Neurospora: its effect on horizontal transfer of mitochondrial plasmids and senescence in natural populations. Curr. Genet. 26, 113–119.
- Roca, M.G., Arlt, J., Jeffree, C.E., and Read, N.D. (2005). Cell biology of conidial anastomosis tubes in *Neurospora crassa*. Eukaryot. Cell 4, 911–919.
- Fleissner, A., Leeder, A.C., Roca, M.G., Read, N.D., and Glass, N.L. (2009).
 Oscillatory recruitment of signaling proteins to cell tips promotes coordinated behavior during cell fusion. Proc. Natl. Acad. Sci. USA 106, 19387–19392.
- Zhao, J., Gladieux, P., Hutchison, E., Bueche, J., Hall, C., Perraudeau, F., and Glass, N.L. (2015). Identification of allorecognition loci in *Neurospora* crassa by genomics and evolutionary approaches. Mol. Biol. Evol. 32, 2417–2432.
- Fujii, S., Kubo, K., and Takayama, S. (2016). Non-self- and self-recognition models in plant self-incompatibility. Nat. Plants 2, 16130.
- Hall, C., Welch, J., Kowbel, D.J., and Glass, N.L. (2010). Evolution and diversity of a fungal self/nonself recognition locus. PLoS ONE 5, e14055.
- Muirhead, C.A., Glass, N.L., and Slatkin, M. (2002). Multilocus self-recognition systems in fungi as a cause of trans-species polymorphism. Genetics 161, 633–641.
- 24. Paoletti, M. (2016). Vegetative incompatibility in fungi: from recognition to cell death, whatever does the trick. Fungal Biol. Rev. 30, 152–162.
- Span, E.A., and Marletta, M.A. (2015). The framework of polysaccharide monooxygenase structure and chemistry. Curr. Opin. Struct. Biol. 35, 93–99
- Hemsworth, G.R., Henrissat, B., Davies, G.J., and Walton, P.H. (2014).
 Discovery and characterization of a new family of lytic polysaccharide monooxygenases. Nat. Chem. Biol. 10, 122–126.
- 27. Harris, P.V., Welner, D., McFarland, K.C., Re, E., Navarro Poulsen, J.C., Brown, K., Salbo, R., Ding, H., Vlasenko, E., Merino, S., et al. (2010). Stimulation of lignocellulosic biomass hydrolysis by proteins of glycoside hydrolase family 61: structure and function of a large, enigmatic family. Biochemistry 49, 3305–3316.
- Fu, C., Iyer, P., Herkal, A., Abdullah, J., Stout, A., and Free, S.J. (2011). Identification and characterization of genes required for cell-to-cell fusion in *Neurospora crassa*. Eukaryot. Cell 10, 1100–1109.
- Corcoran, P., Dettman, J.R., Sun, Y., Luque, E.M., Corrochano, L.M., Taylor, J.W., Lascoux, M., and Johannesson, H. (2014). A global multilocus analysis of the model fungus *Neurospora* reveals a single recent origin of a novel genetic system. Mol. Phylogenet. Evol. 78, 136–147.

- Saenz, G.S., Stam, J.G., Jacobson, D.J., and Natvig, D.O. (2001). Heteroallelism at the het-c locus contributes to sexual dysfunction in outcrossed strains of Neurospora tetrasperma. Fungal Genet. Biol. 34, 123–129.
- Nagy, L.G., Kovács, G.M., and Krizsán, K. (2018). Complex multicellularity in fungi: evolutionary convergence, single origin, or both? Biol. Rev. Camb. Philos. Soc. 93, 1778–1794.
- Kurian, S.M., Di Pietro, A., and Read, N.D. (2018). Live-cell imaging of conidial anastomosis tube fusion during colony initiation in *Fusarium oxy-sporum*. PLoS ONE 13, e0195634.
- Choi, G.H., Dawe, A.L., Churbanov, A., Smith, M.L., Milgroom, M.G., and Nuss, D.L. (2012). Molecular characterization of vegetative incompatibility genes that restrict hypovirus transmission in the chestnut blight fungus *Cryphonectria parasitica*. Genetics 190, 113–127.
- Glass, N.L., and Dementhon, K. (2006). Non-self recognition and programmed cell death in filamentous fungi. Curr. Opin. Microbiol. 9, 553–558.
- Voskoboynik, A., Newman, A.M., Corey, D.M., Sahoo, D., Pushkarev, D., Neff, N.F., Passarelli, B., Koh, W., Ishizuka, K.J., Palmeri, K.J., et al. (2013). Identification of a colonial chordate histocompatibility gene. Science 341, 384–387.
- Hirose, S., Chen, G., Kuspa, A., and Shaulsky, G. (2017). The polymorphic proteins TgrB1 and TgrC1 function as a ligand-receptor pair in *Dictyostelium* allorecognition. J. Cell Sci. 130, 4002–4012.
- Roper, M., Simonin, A., Hickey, P.C., Leeder, A., and Glass, N.L. (2013).
 Nuclear dynamics in a fungal chimera. Proc. Natl. Acad. Sci. USA 110, 12875–12880.
- Simonin, A., Palma-Guerrero, J., Fricker, M., and Glass, N.L. (2012).
 Physiological significance of network organization in fungi. Eukaryot.
 Cell 11, 1345–1352.
- Vogel, H.J. (1956). A convenient growth medium for Neurospora crassa. Microb. Genet. Bull. 13, 42–43.
- Westergaard, M., and Mitchell, H.K. (1947). Neurospora V. A synthetic medium favoring sexual reproduction. Am. J. Bot. 34, 573–577.
- Colot, H.V., Park, G., Turner, G.E., Ringelberg, C., Crew, C.M., Litvinkova, L., Weiss, R.L., Borkovich, K.A., and Dunlap, J.C. (2006). A highthroughput gene knockout procedure for *Neurospora* reveals functions for multiple transcription factors. Proc. Natl. Acad. Sci. USA *103*, 10352– 10257.
- Gonçalves, A.P., Hall, C., Kowbel, D.J., Glass, N.L., and Videira, A. (2014).
 CZT-1 is a novel transcription factor controlling cell death and natural drug resistance in *Neurospora crassa*. G3 (Bethesda) 4, 1091–1102.
- Palma-Guerrero, J., Hall, C.R., Kowbel, D., Welch, J., Taylor, J.W., Brem, R.B., and Glass, N.L. (2013). Genome wide association identifies novel loci involved in fungal communication. PLoS Genet. 9, e1003669.
- Ellison, C.E., Hall, C., Kowbel, D., Welch, J., Brem, R.B., Glass, N.L., and Taylor, J.W. (2011). Population genomics and local adaptation in wild isolates of a model microbial eukaryote. Proc. Natl. Acad. Sci. USA 108, 2831–2836.
- Ellison, C.E., Kowbel, D., Glass, N.L., Taylor, J.W., and Brem, R.B. (2014).
 Discovering functions of unannotated genes from a transcriptome survey of wild fungal isolates. MBio 5, e01046-13.
- Szewczyk, E., Nayak, T., Oakley, C.E., Edgerton, H., Xiong, Y., Taheri-Talesh, N., Osmani, S.A., and Oakley, B.R. (2006). Fusion PCR and gene targeting in Aspergillus nidulans. Nat. Protoc. 1, 3111–3120.
- Bardiya, N., and Shiu, P.K. (2007). Cyclosporin A-resistance based gene placement system for *Neurospora crassa*. Fungal Genet. Biol. 44, 307–314.
- Freitag, M., Hickey, P.C., Raju, N.B., Selker, E.U., and Read, N.D. (2004).
 GFP as a tool to analyze the organization, dynamics and function of nuclei and microtubules in Neurospora crassa. Fungal Genet. Biol. 41, 897–910.
- Schneider, C.A., Rasband, W.S., and Eliceiri, K.W. (2012). NIH Image to ImageJ: 25 years of image analysis. Nat. Methods 9, 671–675.

Please cite this article in press as: Gonçalves et al., Allorecognition upon Fungal Cell-Cell Contact Determines Social Cooperation and Impacts the Acquisition of Multicellularity, Current Biology (2019), https://doi.org/10.1016/j.cub.2019.07.060



- 50. Gonçalves, A.P., Monteiro, J., Lucchi, C., Kowbel, D.J., Cordeiro, J.M., Correia-de-Sá, P., Rigden, D.J., Glass, N.L., and Videira, A. (2014). Extracellular calcium triggers unique transcriptional programs and modulates staurosporine-induced cell death in Neurospora crassa. Microb. Cell 1, 289-302.
- 51. Katoh, K., and Standley, D.M. (2013). MAFFT multiple sequence alignment software version 7: improvements in performance and usability. Mol. Biol. Evol. 30, 772-780.
- 52. Guindon, S., Dufayard, J.F., Lefort, V., Anisimova, M., Hordijk, W., and Gascuel, O. (2010). New algorithms and methods to estimate maximumlikelihood phylogenies: assessing the performance of PhyML 3.0. Syst. Biol. 59, 307-321.
- 53. Kumar, S., Stecher, G., and Tamura, K. (2016). MEGA7: molecular evolutionary genetics analysis version 7.0 for bigger datasets. Mol. Biol. Evol. 33, 1870-1874.
- 54. Quevillon, E., Silventoinen, V., Pillai, S., Harte, N., Mulder, N., Apweiler, R., and Lopez, R. (2005). InterProScan: protein domains identifier. Nucleic Acids Res. 33, W116-W120.
- 55. McGuffin, L.J., Bryson, K., and Jones, D.T. (2000). The PSIPRED protein structure prediction server. Bioinformatics 16, 404-405.
- 56. Elso, C.M., Roberts, L.J., Smyth, G.K., Thomson, R.J., Baldwin, T.M., Foote, S.J., and Handman, E. (2004). Leishmaniasis host response loci (Imr1-3) modify disease severity through a Th1/Th2-independent pathway. Genes Immun. 5, 93-100.



STAR*METHODS

KEY RESOURCES TABLE

REAGENT or RESOURCE	SOURCE	IDENTIFIER
Chemicals, Peptides, and Recombinant Proteins		
Hygromycin B	Thermo Fisher Scientific	10687010
Nourseothricin sulfate	Gold Biotechnology	N-500-100
FM4-64	Thermo Fisher Scientific	T3166
Calcofluor white M2R / Fluorescent Brightener 28	Sigma-Aldrich	F3543
Pluronic F-127	Sigma-Aldrich	P2443
Critical Commercial Assays		
Phire Plant Direct PCR Kit	Thermo Fisher Scientific	F130WH
Deposited Data	'	
Mapped reads for BSA / whole genome resequencing	This paper	https://www.ncbi.nlm.nih.gov/sra (SRA: PRJNA504906)
Computational code for flow cytometry analyses	This paper	https://github.com/gaberosenfield/Glass-Lab-Flow-Cytometry-Analysis
Experimental Models: Organisms/Strains		
Neurospora crassa strains (please see Table S1)	N/A	N/A
Oligonucleotides		
Primers: please see Table S2	N/A	N/A
Recombinant DNA	'	
pCSR-1	Fungal Genetics Stock Center	pCSR1
pMF272	Fungal Genetics Stock Center	pMF272
Software and Algorithms	' ' ' ' ' ' ' ' ' ' ' ' ' ' ' ' ' ' '	
ImageJ	ImageJ	https://imagej.nih.gov/ij/
MATLAB	MathWorks	https://www.mathworks.com/products/matlab.html
FlowJo	FlowJo, LLC	https://www.flowjo.com/
MAFFT	MAFFT	https://mafft.cbrc.jp/alignment/server/index.html
PhyML	ATGC	http://www.atgc-montpellier.fr/phyml/
Mega7	MEGA Software	https://www.megasoftware.net/
InterProScan	EBI	https://www.ebi.ac.uk/interpro/search/ sequence-search
MEMSAT3/PSIPRED	UCL	http://bioinf.cs.ucl.ac.uk/psipred/

LEAD CONTACT AND MATERIALS AVAILABILITY

Further information and requests for resources and reagents should be directed to and will be fulfilled by the Lead Contact, N. Louise Glass (Lglass@berkeley.edu). Strains and plasmids generated in this study are available from the Fungal Genetics Stock Center (http://www.fgsc.net/) and/or the Lead Contact.

EXPERIMENTAL MODEL AND SUBJECT DETAILS

Neurospora crassa

Vogel's minimal medium (VMM; with 2% sucrose and 1.5% agar) was employed for routine cultivation of *N. crassa* [39]. Asexual spores were obtained by growing strains in glass tubes with slanted VMM for 2 days in the dark, 30°C, followed by 4-6 more days at room temperature. For matings, synthetic cross medium (SC; with 1% sucrose and 1.5% agar) was used [40]. Briefly, a female parent strain that had been grown on SC until protoperithecia were observed – usually 8-10 days after inoculation – was fertilized with a conidial suspension of a male parent strain and grown for an additional 8-10 days until ascospores had been shot to the lid of

Please cite this article in press as: Gonçalves et al., Allorecognition upon Fungal Cell-Cell Contact Determines Social Cooperation and Impacts the Acquisition of Multicellularity, Current Biology (2019), https://doi.org/10.1016/j.cub.2019.07.060



the Petri dish. Strains used in this study are listed in Table S1. Deletion strains were constructed in a FGSC2489 genetic background [41]. Isolates from a Louisiana population have been previously described [16, 20, 42-45]. Genotypes were confirmed by PCR (Phire Plant Direct PCR Kit; Thermo Fisher Scientific) and/or Sanger sequencing. All experiments were performed at least in quadruplicates.

METHOD DETAILS

PCR

Fusion PCR [46] was employed to generate double and triple deletion mutants. For the ΔNCU01380ΔNCU01382 double mutant, a ΔNCU01382 deletion was introduced in a ΔNCU01380 strain. A Pfu-based PCR strategy was used for site-directed mutagenesis of NCU01380. Key primers are described in Table S2.

Transformation

Transformations were performed via electroporation based on pCSR-1 [47] or pMF272 [48] vectors. Conidia from one-week cultures of the recipient strain were harvested with ice-cold 1M sorbitol. After two washes, cells were resuspended in 90 µl 1M sorbitol and mixed with 10 µl containing of 1-2 µg of DNA. The mixture was transferred to 1 mm gap cuvettes and electroporated using a Gene Pulser II (Bio-Rad) with the following settings: 1.5 kV, 25 μF, 600 ohms. Ice-cold sorbitol (900 μI) was guickly added to the sample, mixed with top agar medium (VMM with 1% agar, 1M sorbitol and a mixture of 2% sorbose, 0.05% glucose, 0.05% fructose as the carbon source; the three last components added after autoclaving) that was kept at ~55°C and overlaid on previously prepared plates containing solidified bottom agar medium (identical to top agar but without sorbitol and with agar at a concentration of 1.5%) (containing 200 μg/ml hygromycin B (Thermo Fisher Scientific) or 80 μg/ml nourseothricin sulfate (Gold Biotechnology), when necessary for selection of transformants).

Epifluorescence and confocal microscopy

Conidia were diluted to 1.5 × 10⁷ cells/ml. Strains bearing superfolder GFP (sGFP, hereafter referred as GFP) under the control of the ccg-1 promoter or strains expressing SOFT-GFP or MAK-2-GFP were used to assess cell fusion [19]. Other strains were stained with 2 µM FM4-64 (Thermo Fisher Scientific) for 15 mins in the dark. The FM4-64-stained cells were washed twice with sterile and H₂O and mixed in a 1:1 proportion with the GFP-expressing cells. Eighty µl of the strain mixture were spread onto 5 cm VMM plates and incubated at 30°C in the dark for 3.5-4 hr. In some experiments, 7 µl of 5 mg/ml calcofluor white M2R (Sigma-Aldrich) was added to the sample. Fluorescence microscopy was performed on a Zeiss Axioskop 2 or on a Leica SD6000 confocal microscope equipped with a Yokogawa CSU-X1 spinning disk head or on a Zeiss LSM710. Images were analyzed using ImageJ [49]. For SOFT and MAK-2 oscillation experiments, mean pixel intensity was measured at the fusion spot and normalized with a region not involved in contact [19]. For hyphal fusion experiments, 3 µl of 10⁸ cells/ml were inoculated 5 mm apart on the center of a VMM plate.

Flow cytometry

Cultures were prepared as for microscopy, but 20% Pluronic F-127 (Sigma-Aldrich) [15] was used instead of agar. After 4 hr of incubation, samples were placed at -20°C for 10 mins, allowing for liquefaction of the Pluronic, followed by two washes with 1x PBS and final resuspension in 1x PBS containing 0.1 $\mu g/\mu l$ propidium iodide (PI) for cell death measurements. Cell death frequencies for at least 10,000 germlings were recorded on a BD LSR Fortessa X-20. Ungerminated conidia were run in parallel to allow gating of ungerminated from germinated spores. PI quantification was obtained using MATLAB (MathWorks). A computational code that automatically gates out ungerminated spores, recognizes fluorescence peaks and employs an exponential decay curve to fit and correct the data was used (Figure S2). For germination measurements, 20,000 total events were recorded and FlowJo (FlowJo, LLC) was used for analyses.

Transmission electron microscopy

Liquid VMM was inoculated with conidia from the indicated strains at a concentration of 10⁶ cells/ml and incubated for 5 hr at 30°C (shaking at 200 rpm for 2.5 hr and without standing for 2.5 hr). After pelleted by centrifugation, cells were fixed with 2% glutaraldehyde, 4% paraformaldehyde, 0.04 M phosphate buffer (pH 7.0), followed by 2% KMnO₄ treatment. Samples were then dehydrated using a graded ethanol series before embedding the samples in resin.

For evaluation of radial growth [50], a 20 µl inoculum containing 5x10⁴ conidia was spotted on the center of 14.2 cm diameter Petri dishes and grown at 30°C, in constant dark. The colony diameter was recorded twice a day.

Bulk segregant analysis (BSA)

BSA followed by whole genome resequencing was performed as previously described [16]. Equal amounts of genomic DNA from 50 segregants in each pool were combined and used for library preparation.

Please cite this article in press as: Gonçalves et al., Allorecognition upon Fungal Cell-Cell Contact Determines Social Cooperation and Impacts the Acquisition of Multicellularity, Current Biology (2019), https://doi.org/10.1016/j.cub.2019.07.060



Bioinformatics

Phylogenetic trees were constructed from MAFFT alignments [51] using PhyML [52] or Mega7 [53]. The mean evolutionary diversity was calculated from MAFFT alignments using Mega7 [53]. Conserved domains were identified manually or by using InterProScan [54]. The topography of NCU01382 was predicted using MEMSAT3/PSIPRED [55].

QUANTIFICATION AND STATISTICAL ANALYSIS

Prism (Graphpad Software) was used for the statistical analyses indicated in each figure, except for Figure 5B, in which the CGGC permutation test was used [56]. Data are presented as mean and standard deviation of multiple independent replicates and individual data points are shown.

DATA AND CODE AVAILABILITY

Mapped reads for each pool of DNA used for whole genome resequencing and bulk segregant analysis are available at https://www. ncbi.nlm.nih.gov/sra (SRA: PRJNA504906). The computational code used in this study for flow cytometry analyses (see also Figure S2) is available at https://github.com/gaberosenfield/Glass-Lab-Flow-Cytometry-Analysis.

Current Biology, Volume 29

Supplemental Information

Allorecognition upon Fungal Cell-Cell
Contact Determines Social Cooperation
and Impacts the Acquisition of Multicellularity

A. Pedro Gonçalves, Jens Heller, Elise A. Span, Gabriel Rosenfield, Hung P. Do, Javier Palma-Guerrero, Natalia Requena, Michael A. Marletta, and N. Louise Glass

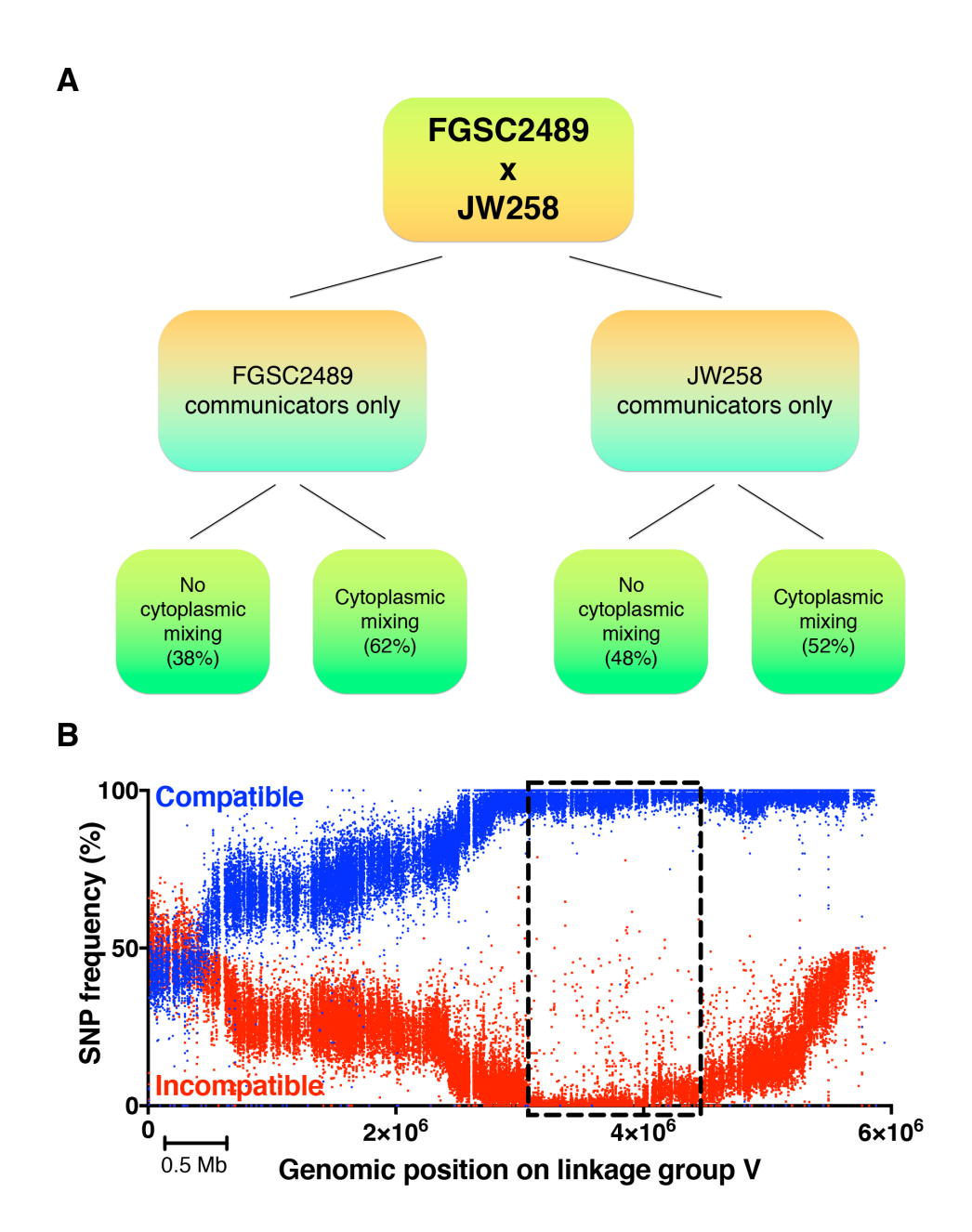


Figure S1. Summary of the bulk segregant analysis and re-sequencing employed to identify the genetic basis of the cell wall arrest phenotype. Related to Figures 1 and 3. (A) FGSC2489 was crossed with the wild isolate JW258 and the progeny was initially screened for their ability to communicate with either parental strains [S1]. Cytoplasmic mixing was subsequently evaluated within each of the communication groups and the resulting percentages of progeny that showed cytoplasmic mixing or not are shown. (B) Whole genome resequencing of two pools of DNA obtained from progeny strains in the incompatible (38%; red) and compatible (62%; blue) groups of FGSC2489 communicators revealed a 1Mb region on chromosome V that showed 100% SNP segregation (highlighted by the dashed rectangle).

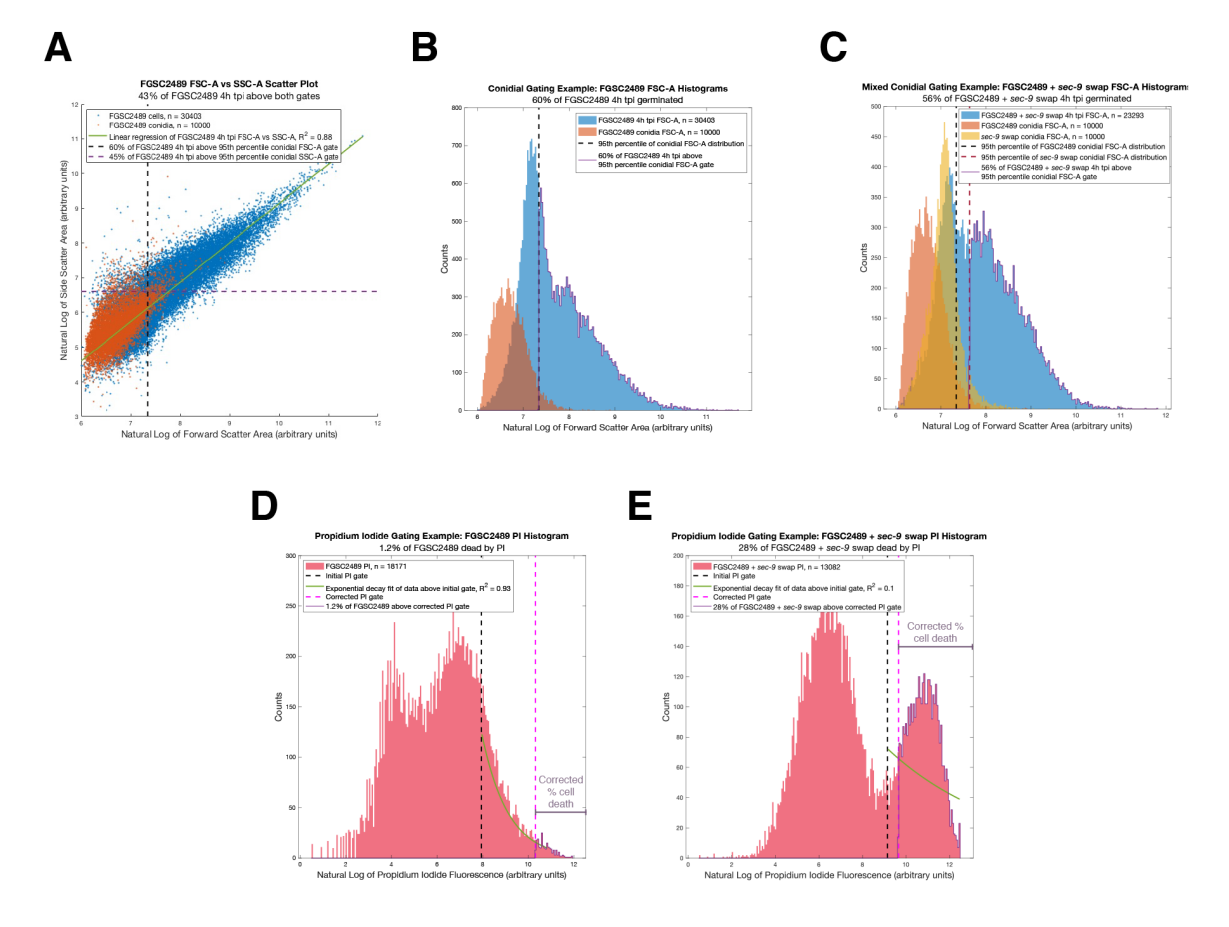


Figure S2. Automatic gating of germinated/ungerminated spores and quantification of cell death by flow cytometry. Related to Figures 1, 4 and 5. (A) Natural log of forward scatter area (FSC-A) versus natural log of side scatter area (SSC-A) of a representative experiment showing FGSC2489 ungerminated conidia (red) and the same conidia grown for 4 hrs as described in the Methods section (blue) with linear regression and germination gates. Gates were drawn at the 95th percentile of conidial FSC-A & SSC-A distributions (dashed lines). FSC-A was used for gating out conidia in subsequent analyses because forward scatter area is proportional to cell size, which increases as conidia germinate. SSC-A measures cell refractivity, which has a less obvious relationship with germination. FSC-A and SSC-A are correlated ($R^2 = 0.88$), such that using a two-dimensional gate (FSC-A and SSC-A, in this example, resulted in 43% of germination) is only slightly different than the germination rate obtained with using the more restrictive one-dimensional gate (SSC-A, in this example, resulted in 45% germination). Using the FSC-A one-dimensional gate resulted in 60% germination. (B) Histogram of the natural log of FSC-A of FGSC2489 ungerminated conidia (red) and the same conidia grown for 4 hours as described in the Methods section (blue), with germination gate. Gate drawn at the 95th percentile of conidial FSC-A distribution, yielded a 60% germination rate in this example. Data from cells considered germinated are outlined in purple. (C) Histogram of the natural log of FSC-A of FGSC2489 ungerminated conidia (red), 'sec-9 swap' ungerminated conidia (yellow) and mixed FGSC2489+'sec-9 swap' conidia grown for 4 hrs as described in the Methods section (blue), with germination gates. Gates drawn at the 95th percentiles of conidial FSC-A distributions. For mixed samples, the more restrictive 95th percentile conidial gate was used. In this example, the 'sec-9 swap' conidial gate was used and yielded a 56% germination rate. Data from cells

considered germinated are outlined in purple. (D) Histogram of the natural log of propidium iodide (PI) fluorescence area of germinated FGSC2489 cells with fluorescence gates and exponential decay fit. The initial gate (black dotted line) is defined using two-level Otsu's thresholding method [S2], with the higher threshold becoming the initial gate. Data above the initial gate is fit with an exponential decay curve, and the correlation coefficient is used to correct the percentage of the data above the initial gate according to the following formula: (% above initial gate) x (1 - correlation coefficient) = (corrected % cell death). In this example, 16.8% of germinated FGSC2489 cells are above the initial gate and $R^2 = 0.93$ for the exponential fit; this resulted in 1.2% corrected cell death. Data from events above the corrected gate are outlined in purple. (E) Histogram of the natural log of PI fluorescence area of germinated mixed FGSC2489+'sec-9 swap' cells with fluorescence gates & exponential decay fit. In this example, 31.8% of germinated mixed FGSC2489+'sec-9 swap' cells were above the initial gate and R^2 = 0.1 for the exponential fit; this resulted in 28% corrected cell death. Data from events above the corrected gate are outlined in purple. The percentage of corrected cell death is indicated as 'Fusion/death score' in various panels of Figures 1, 4 and 5. tpi = time post-inoculation. Repository for analyses: https://github.com/gaberosenfield/Glass-Lab-Flow-Cytometry-Analysis.

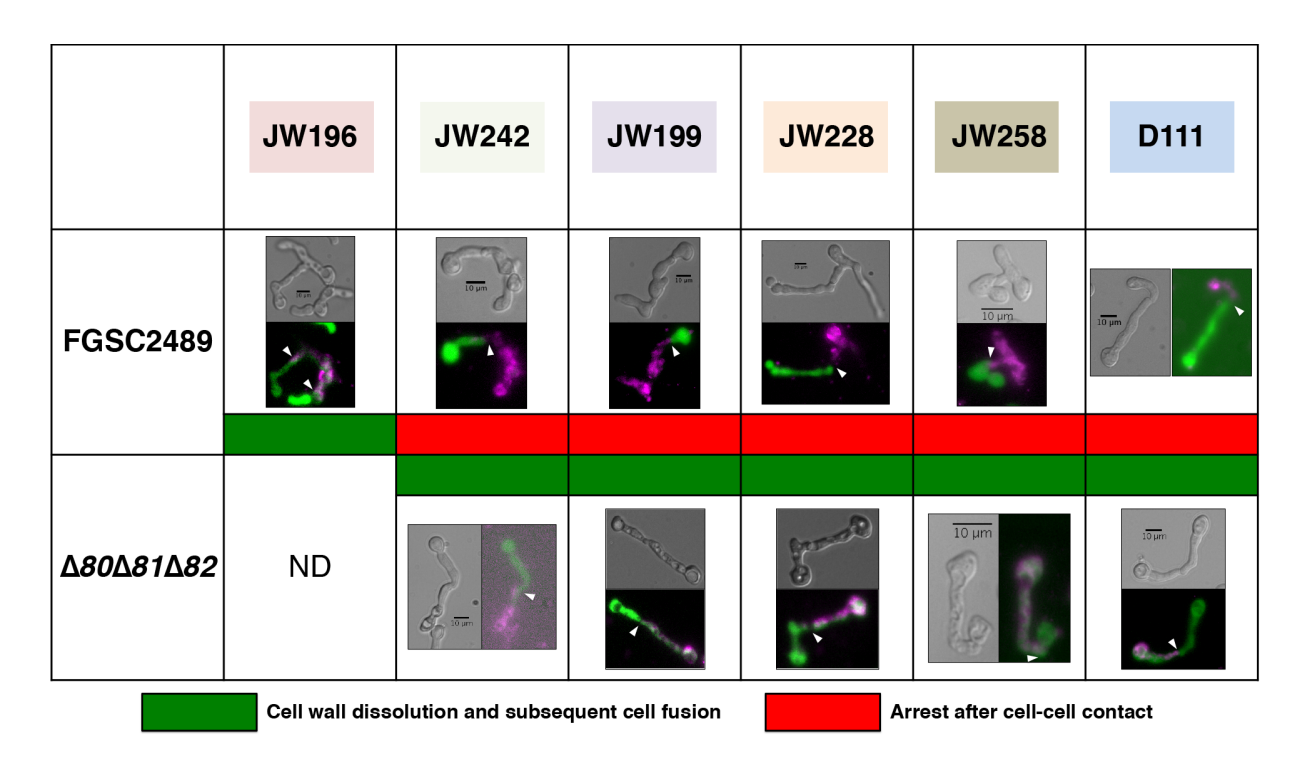


Figure S3. Cell fusion analyses of selected wild isolates. Related to Figure 3. The ability to disassemble the cell wall at the zone of interaction and subsequently to fuse was tested for combinations of FGSC2489-background strains with selected wild isolates. Wild isolates were stained with FM4-64. FGSC2489-background strains expressed cytoplasmic GFP. For JW199 and JW228 pairings, FGSC2489 was employed; for the JW196, JW258 and JW242 pairings, the FGSC2489-background strain harbored a $\Delta doc-1\Delta doc-2$ double deletion; for the D111 pairing, the FGSC2489-background strain harbored a $\Delta doc-1\Delta doc-2$ double deletion and expressed doc-1 and doc-2 alleles from P4471. In the bottom panel, all FGSC2489-background strains harbored a $\Delta cwr-1\Delta$ NCU01381 $\Delta cwr-2$ triple deletion. ND, not determined. Arrowheads indicate the zone of interaction between cells. Colored rectangles on the strain name have correspondence to Figure 3A.

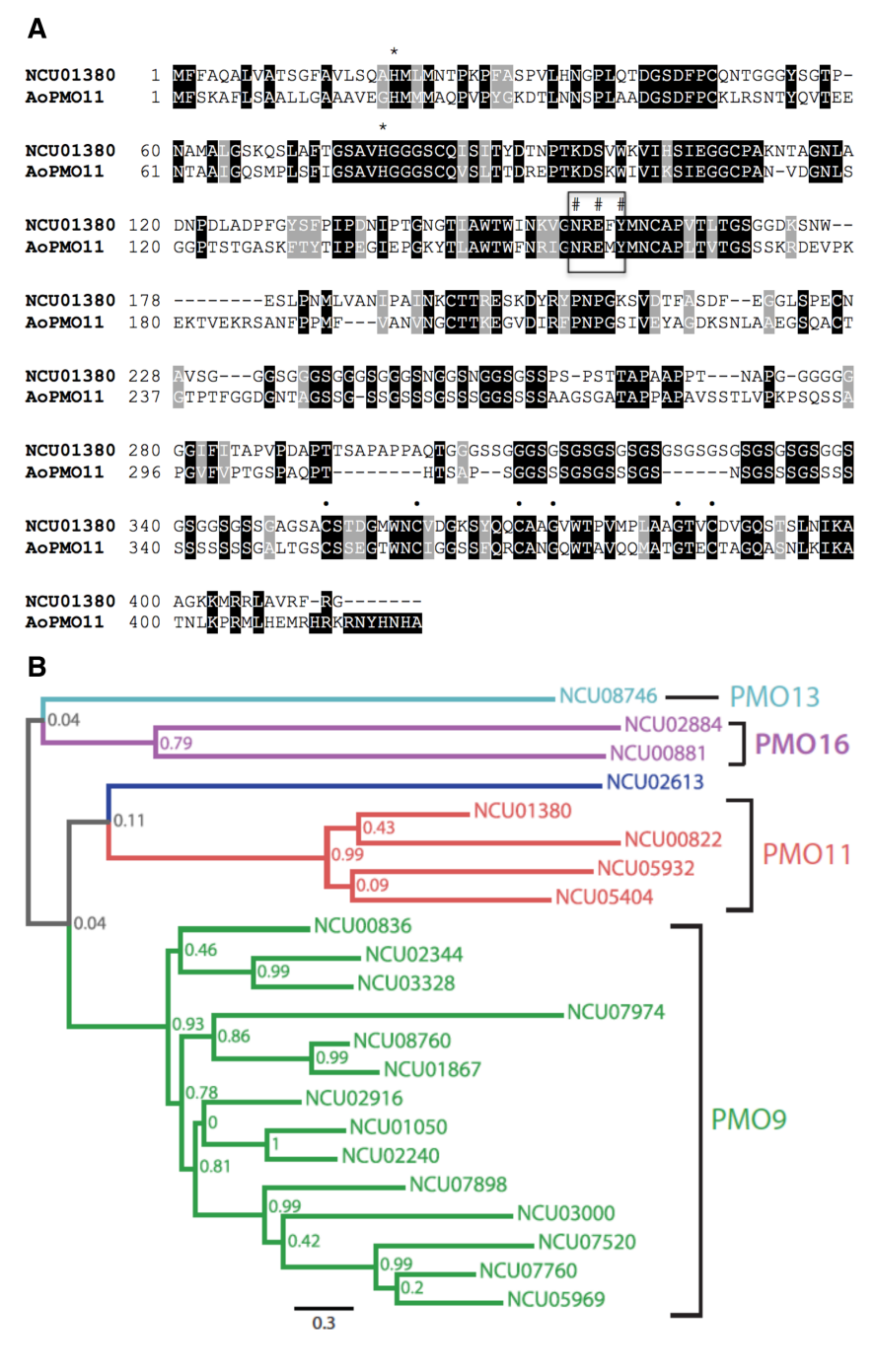


Figure S4. NCU01380 encodes a predicted polysaccharide monooxygenase. Related to Figure 3. (A) Protein sequence alignment of NCU01380 and *Aspergillus oryzae* PMO11 (Uniprot ID: Q2UA85_ASPOR). *, conserved histidine residues that form the histidine brace that coordinates copper ions. A rectangle highlights the hydrogen-bonding motif, with conserved residues marked with #, which includes the conserved Y residue; •, conserved cysteines and glycines in the predicted carbohydrate-binding module. (B) The predicted proteome of *N. crassa* was surveyed for the presence of PMOs and a maximum likelihood tree was built. Bootstrap values for each node are shown. Different clusters were called PMO9, PMO11, PMO16 and PMO13.

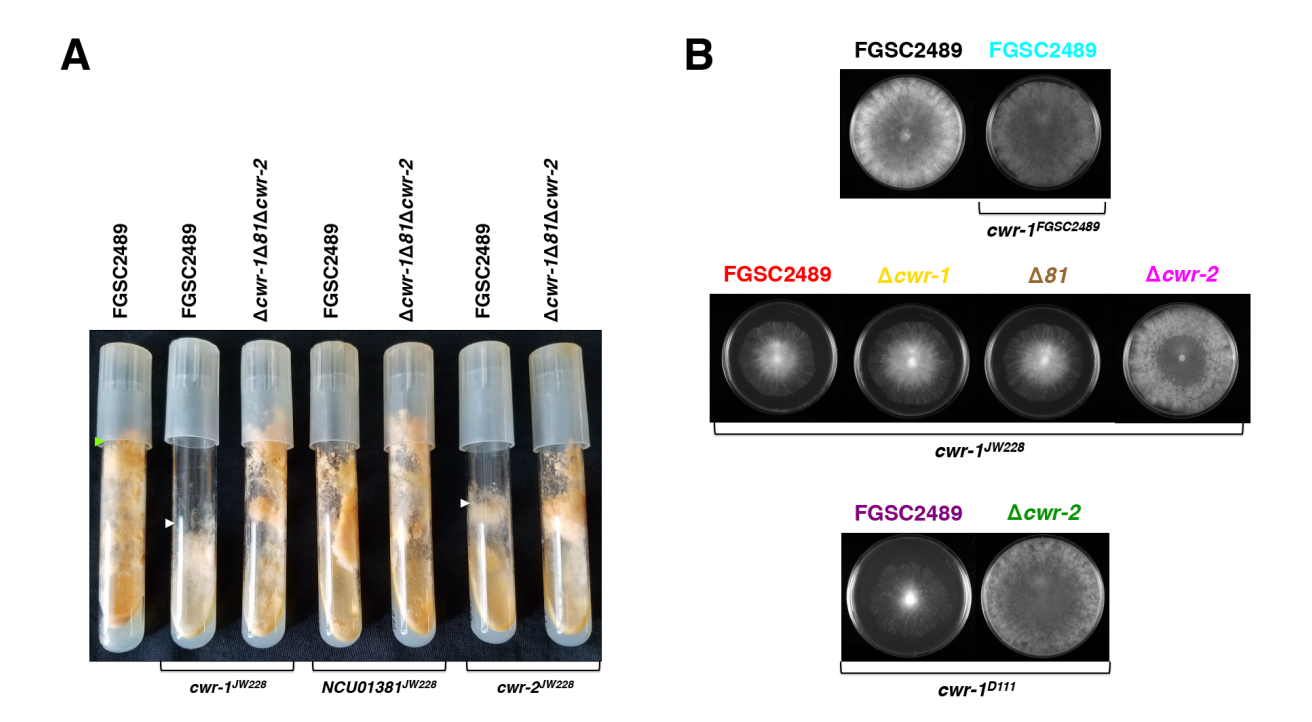


Figure S5. Expression of *cwr-1*^{JW228} or *cwr-2*^{JW228} in FGSC2489 results in morphological and fusion defects. Related to Figure 5. (A) Asexual development in slant tubes was evaluated after 7 days. Genes indicated below the tubes were introduced into the strain background indicated above the tubes. White arrowheads indicate reduced aerial hyphae *versus* the parental FGSC2489 strain (green arrowhead). In the $\Delta cwr-1$ Δ NCU01381 $\Delta cwr-2$ strain, the expression of cwr-1^{JW228} or cwr-2^{JW228} does not result in reduced aerial hyphae. (B) Spores from indicated strains expressing cwr-1 alleles specified on the bottom were inoculated on the center of a Petri dish and photographs of the colonies were taken after 48 hrs of growth.

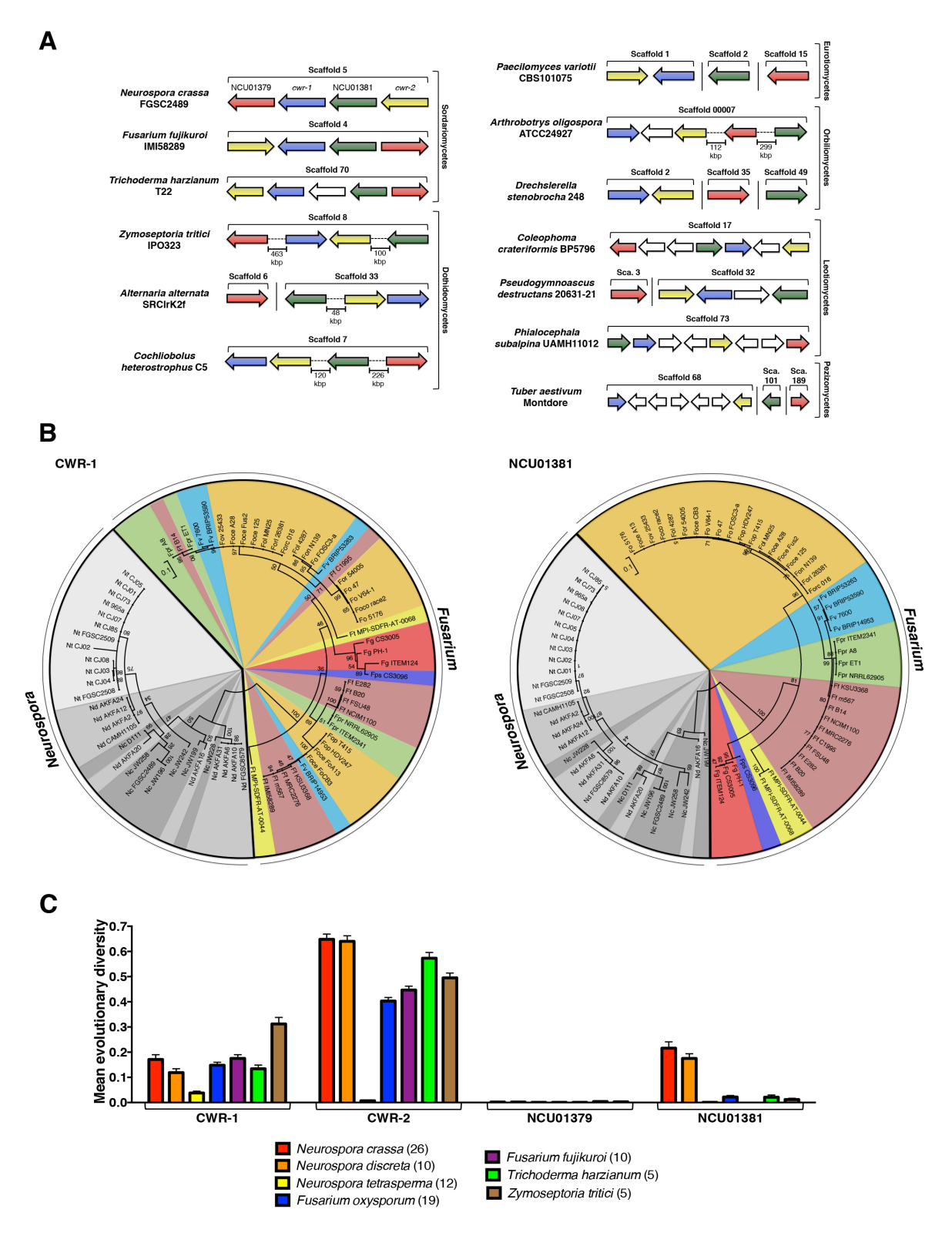


Figure S6. Distant CWR orthologs present features of balancing selection and convergent evolution. Related to Figure 6. (A) Genomic situation of *cwr-1* (blue), *cwr-2* (yellow), NCU01379 (red) and NCU01381 (green) orthologs in various fungal strains of the

Pezizomycotina subphylum. (B) The amino acid sequence of orthologs of CWR-1 and NCU01381 from the indicated isolates were used to build maximum likelihood phylogenetic trees. Bootstrap results (from 100 bootstrap replicates) are indicated at the nodes in grey. Strains of the same species are shaded with identical colors: light grey, *N. tetrasperma*; medium grey, *N. discreta*; dark grey, *N. crassa*; light yellow, *F. tricinctum*; yellow, *F. oxysporum*; pink, *F. fujikuroi*; red, *F. graminearum*; green, *F. proliferatum*; blue, *F. verticillioides*; purple, *F. pseudograminearum*. Note the mixed colors on several branches for CWR-1, indicating transspecies polymorphisms. TSP were also observed for NCU01381, but was unique to *Neurospora*. (C) The mean evolutionary diversity (MED) for each gene ± standard error (100 bootstrap replicates; JTT matrix-based model) was calculated for each of the indicated species. The number of alleles available for each species is indicated between parentheses.

Name	Genotype/Notes	Source	Fusion/ death score #
FGSC2489 (74-OR23-IV)	-	FGSC	2.05 ± 0.38
FGSC2489/GFP	his-3::Pccg-1-gfp	FGSC	ND
Seg11	Progeny of FGSC2489 x JW258	*	2.49 ± 0.46
Seg3	Progeny of FGSC2489 x JW258	*	3.54 ± 2.68
ΔΔsec-9 (sec-9 swap)	Δplp-1(NCU09244)Δplp-2(NCU09244); sec- 9(NCU09243) ^{JW199}	[S3]	3.37 ± 1.89
SO-GFP	his-3::Pccg-1-NCU02794-gfp	[S4]	ND
MAK-2-GFP	his-3::Pccg-1-NCU02393-gfp	[S4]	ND
Δcwr - $1\Delta 81\Delta cwr$ - 2	ΔNCU01380ΔNCU01381ΔNCU01382	*	2.74 ± 2.20
Δcwr-1Δ81Δcwr-2/GFP	ΔNCU01380ΔNCU01381ΔNCU01382; <i>his-</i> 3::Pccg-1-gfp	*	ND
Δcwr-1/GFP	ΔNCU01380; his-3::Pccg-1-gfp	*	ND
Δcwr-1; ΔΔsec-9	ΔNCU01380; Δ <i>plp-1(NCU09244)</i> Δ <i>plp-2(NCU09244)</i> ; sec-9(NCU09243) ^{JW199}	*	2.74 ± 2.69
Δ81/GFP	ΔNCU01381; his-3::Pccg-1-gfp	*	ND
Δ81; ΔΔsec-9	ΔNCU01381; Δ <i>plp-1(NCU09244)</i> Δ <i>plp-2(NCU09244)</i> ; sec-9(NCU09243) ^{JW199}	*	1.74 ± 0.91
Δcwr-2/GFP	ΔNCU01382; his-3::Pccg-1-gfp	*	ND
Δ <i>cwr</i> -2; ΔΔ <i>sec</i> -9	ΔNCU01382; Δ <i>plp-1(NCU09244)</i> Δ <i>plp-2(NCU09244)</i> ; sec-9(NCU09243) ^{JW199}	*	7.69 ± 5.67
Δcwr-1Δ81/GFP	ΔNCU01380ΔNCU01381; his-3::Pccg-1-gfp	*	ND
Δcwr - $I\Delta 81$; $\Delta \Delta sec$ - 9	ΔNCU01380ΔNCU01381; Δ <i>plp-</i> 1(NCU09244)Δ <i>plp-2</i> (NCU09244); sec- 9(NCU09243) ^{JW199}	*	4.47 ± 5.38
Δ81Δ <i>cwr-2</i> /GFP	ΔNCU01381ΔNCU01382; his-3::Pccg-1-gfp	*	ND
Δ81Δ <i>cwr-2</i> ; ΔΔ <i>sec-9</i>	ΔNCU01381ΔNCU01382; Δ <i>plp-</i> 1(NCU09244)Δ <i>plp-2</i> (NCU09244); sec- 9(NCU09243) ^{JW199}	*	4.35 ± 3.47
Δcwr-1Δcwr-2/GFP	ΔNCU01380ΔNCU01382; his-3::Pccg-1-gfp	*	ND
Δcwr - $I\Delta cwr$ - 2 ; $\Delta \Delta sec$ - 9	ΔNCU01380ΔNCU01382; Δ <i>plp-</i> 1(NCU09244)Δ <i>plp-2</i> (NCU09244); sec- 9(NCU09243) ^{JW199}	*	1.91 ± 0.96
Δcwr - $I\Delta 81\Delta cwr$ - 2 ; $\Delta \Delta sec$ - 9	ΔNCU01380ΔNCU01381ΔNCU01382; Δplp-1(NCU09244)Δplp-2(NCU09244); sec- 9(NCU09243) ^{JW199}	*	3.28 ± 1.26
Δ <i>cwr-1</i> Δ81Δ <i>cwr-2</i> ; 81- GFP	ΔNCU01380ΔNCU01381ΔNCU01382; <i>his-</i> 3::Pccg-1-NCU01381-gfp	*	ND
Δ <i>cwr-1</i> Δ81Δ <i>cwr-2</i> ; 81- GFP; ΔΔ <i>sec-9</i>	ΔNCU01380ΔNCU01381ΔNCU01382; ; his-3::Pccg-1-NCU01381-gfp; Δplp-	*	1.99 ± 0.73

	1(NCU09244)Δplp-2(NCU09244); sec- 9(NCU09243) ^{JW199}		
Δcwr - $I\Delta 81\Delta cwr$ - 2 ; cwr - I^{JW228}	ΔNCU01380ΔNCU01381ΔNCU01382; <i>his</i> -3::Ptef-1-NCU01380 ^{JW228}	*	2.73 ± 1.75
Δ <i>cwr-1</i> Δ81Δ <i>cwr-2</i> ; 81 ^{JW228}	ΔNCU01380ΔNCU01381ΔNCU01382; his- 3::Ptef-1-NCU01381 ^{JW228}	*	2.13 ± 1.22
Δcwr - $I\Delta 81\Delta cwr$ - 2 ; cwr - 2^{JW228}	ΔNCU01380ΔNCU01381ΔNCU01382; <i>his-</i> 3::Ptef-1-NCU01382 ^{JW228}	*	1.55 ± 1.26
Δcwr - $I\Delta 81\Delta cwr$ - 2 ; cwr - I^{wt}	ΔNCU01380ΔNCU01381ΔNCU01382; <i>his-</i> 3::PNCU01380-NCU01380	*	1.83 ± 0.69
Δcwr - $1\Delta 81\Delta cwr$ - 2 ; cwr - 1^{Y159A}	ΔNCU01380ΔNCU01381ΔNCU01382; <i>his-</i> 3::PNCU01380-NCU01380(475TAC> GCT)	*	1.84 ± 0.93
FGSC2489; cwr-1 ^{FGSC2489}	<i>csr-1</i> :: Pgpd-1-NCU01380 ^{FGSC2489}	*	ND
FGSC2489; <i>csr-1</i> :: <i>cwr- I</i> ^{JW228}	csr-1:: Pgpd-1-NCU01380 ^{JW228}	*	0.76 ± 0.50
Δcwr-1; csr-1::cwr-1 ^{JW228}	ΔNCU01380; <i>csr-1</i> :: P <i>gpd-1</i> - NCU01380 ^{JW228}	*	ND
ΔNCU01381; csr-1::cwr- 1 ^{JW228}	ΔNCU01381; csr-1:: Pgpd-1- NCU01380 ^{JW228}	*	ND
Δcwr-2; csr-1::cwr-1 ^{JW228}	ΔNCU01382; <i>csr-1</i> :: P <i>gpd-1</i> - NCU01380 ^{JW228}	*	5.57 ± 5.26
Δcwr - $1\Delta 81$; csr - 1 :: cwr - 1 ^{JW228}	ΔNCU01380ΔNCU01381; csr-1:: Pgpd-1- NCU01380 ^{JW228}	*	ND
$\Delta 81\Delta cwr$ -2; csr -1:: cwr - 1^{JW228}	ΔNCU01381ΔNCU01382; csr-1:: Pgpd-1- NCU01380 ^{JW228}	*	ND
$\Delta cwr-1\Delta cwr-2$; $csr-1$:: $cwr-1^{JW228}$	ΔNCU01380ΔNCU01382; csr-1:: Pgpd-1- NCU01380 ^{JW228}	*	ND
Δcwr - $1\Delta 81\Delta cwr$ - 2 ; csr - 1 :: cwr - 1 ^{JW228}	ΔNCU01380ΔNCU01381ΔNCU01382; <i>csr-1</i> :: P <i>gpd-1</i> -NCU01380 ^{JW228}	*	ND
Δcwr -1; cwr -2 ^{JW228}	ΔNCU01380; his-3:: Ptef-1-NCU01382 ^{JW228}	*	ND
FGSC2489; <i>cwr-1</i> ^{D111}	<i>csr-1</i> :: P <i>gpd-1</i> -NCU01380 ^{D111}	*	ND
Δcwr -2; cwr - I^{D111}	ΔNCU01382; csr-1:: Pgpd-1-NCU01380 ^{D111}	*	ND
FGSC2489; <i>csr-1</i> :: <i>cwr-</i> 1 ^{JW228} /GFP	csr-1:: Pgpd-1-NCU01380 ^{FGSC2489} ; his- 3::Pccg-1-gfp	*	ND
Δcwr-2; csr-1::cwr- 1 ^{JW228} /GFP	ΔNCU01382; <i>csr-1</i> :: Pgpd-1- NCU01380 ^{FGSC2489} ; <i>his-3</i> ::Pccg-1-gfp	*	ND
FGSC2489; <i>csr-1::cwr-1^{JW228}</i> ; ΔΔ <i>sec-9</i>	csr-1:: Pgpd-1-NCU01380 ^{FGSC2489} ; Δplp- 1(NCU09244)Δplp-2(NCU09244); sec- 9(NCU09243) ^{JW199}	*	2.05 ± 1.67
Δcwr -2; csr -1:: cwr -1 ^{JW228} ; $\Delta \Delta sec$ -9	ΔNCU01382; csr-1:: Pgpd-1- NCU01380 ^{FGSC2489} ; Δplp- 1(NCU09244)Δplp-2(NCU09244); sec- 9(NCU09243) ^{JW199}	*	6.28 ± 1.53
hH1-dsRed	his-3::Pccg-1-NCU06863-dsRed; rid-1	[S5]	ND
JW258	Wild isolate	[S6]	nd
JW199	Wild isolate	[S6]	2.11 ± 0.65

JW228	Wild isolate	[S6]	ND
JW242	Wild isolate	[S6]	ND
JW196	Wild isolate	[S6]	ND
D111	Wild isolate	[S6]	ND
Δdoc -1 Δdoc -2/GFP	ΔNCU07191ΔNCU07192; his-3::Pccg-1-gfp	[S1]	ND
Δdoc -1 Δdoc -2; doc -1 doc - 2^{CG3} /GFP	ΔNCU07191ΔNCU07192; his-3::doc-1 P4471 doc-2 ^{P4471} ; Pccg-1-gfp	[S1]	ND
Δcwr - $1\Delta 81\Delta cwr$ - $2\Delta doc$ - $1\Delta doc$ - $2/GFP$	ΔNCU01380ΔNCU01381ΔNCU01382ΔNC U07191ΔNCU07192; his-3::Pccg-1-gfp		ND
Δcwr - $1\Delta 81\Delta cwr$ - $2\Delta doc$ - $1\Delta doc$ - 2 ; doc - $1doc$ - 2 ^{CG3} /GFP	ΔNCU01380ΔNCU01381ΔNCU01382ΔNC U07191ΔNCU07192; his-3::doc-1 ^{P4471} doc- 2 ^{P4471} ; Pccg-1-gfp	*	ND
FGSC2489; his-3::cwr-1 ^{JW228}	his-3::Ptef-1-NCU01380 ^{JW228}	*	ND
FGSC2489; 81 ^{JW228}	his-3::Ptef-1-NCU01381 ^{JW228}	*	ND
FGSC2489; 81 ^{JW228} /GFP	his-3::Ptef-1-NCU01381 ^{JW228} ; csr-1::Pccg-1-gfp		ND
FGSC2489; cwr-2 ^{JW228}	his-3::Ptef-1-NCU01382 ^{JW228}	*	ND

FGSC: Fungal Genetics Stock Center [S7]; *: This study. # Fusion/death score, as determined by flow cytometry, of the respective strains grown alone is shown as the mean ± standard deviation. ND: Not determined.

Table S1. Neurospora crassa strains. Related to Figures 1-5.

Name	Sequence	Purpose
hph F	CGGAGACAGAAGATGATATTGAAGGAGC	Hygromycin B resistance cassette
hph R	GTTGGAGATTTCAGTAACGTTAAGTGGAT	Hygromycin B resistance cassette
Nat F	ctagetgattetggagtgace	Nourseothricin sulfate resistance cassette
Nat R	agettgeaaattaaageettegage	Nourseothricin sulfate resistance cassette
NCU01382_5'_fl ank_f	ggccagactaagttatgtcggagg	Generation of ΔNCU01380 ΔNCU01381 ΔNCU01382 and ΔNCU01381 ΔNCU01382; flanking fragment
NCU01382_5'_f usion_r	GCTCCTTCAATATCATCTTCTGTCTCCGgcc atcttgccgtggatcctg	Generation of ΔNCU01380 ΔNCU01381 ΔNCU01382 and ΔNCU01381 ΔNCU01382; flanking fragment
NCU01380_3'_f usion_f	ATCCACTTAACGTTACTGAAATCTCCAACa ccctgagctttatgtgacc	Generation of ΔNCU01380 ΔNCU01381 ΔNCU01382 and ΔNCU01380 ΔNCU01381; flanking fragment
NCU01380_3'_fl ank_r	aagctctattggcatggagg	Generation of ΔNCU01380 ΔNCU01381 ΔNCU01382 and ΔNCU01380 ΔNCU01381; flanking fragment
NCU01382_5'_f _nested	ggtatcggtaaactcgttgggttg	Generation of ΔNCU01380 ΔNCU01381 ΔNCU01382 and ΔNCU01380 ΔNCU01382 *; fusion PCR
NCU01380_3_r _nested	gcaagttagttacgatgagcgccag	Generation of ΔNCU01380 ΔNCU01381 ΔNCU01382; fusion PCR
NCU01381_5'_fl ank_f	gaacgacagcgaagtcgtg	Generation of ΔNCU01380 ΔNCU01381; flanking fragment
NCU01381_5'_f usion r	GCTCCTTCAATATCATCTTCTGTCTCCGgag tgaagccgaggagtg	Generation of ΔNCU01380 ΔNCU01381; flanking fragment
NCU01381_5'_f _nested	ggatatgtccaataagcgattg	Generation of ΔNCU01380 ΔNCU01381; fusion PCR
NCU01381_3'_f usion_f	ATCCACTTAACGTTACTGAAATCTCCAAC gtctaaactttcttcgccgag	Generation of ΔNCU01381 ΔNCU01382; flanking fragment
NCU01381_3'_fl ank_r	gataattcggatcccagcg	Generation of ΔNCU01381 ΔNCU01382; flanking fragment
NCU01381_3'_r _nested	gttgactggttgctgaacg	Generation of ΔNCU01381 ΔNCU01382; fusion PCR
NCU01382_aR(Nat)	gtcactccagaatcagctagGAAGGACAGCTTCAAA CT	Generation of ΔNCU01380 ΔNCU01382; flanking fragment *
NCU01382_cF(Nat)	aaggetttaatttgcaagetAATAAGCGATTGACTTG CAC	Generation of ΔNCU01380 ΔNCU01382; flanking fragment *
NCU01382_cR	TGAAGCCGAGGAGTGTTAGCA	Generation of ΔNCU01380 ΔNCU01382; flanking fragment *
NCU01382_cnes ted	GGTGATATCAATAAATGACTCGGAC	Generation of ΔNCU01380 ΔNCU01382; fusion PCR *
80JW228_FXbaI	ACAtctagaATGCACTTCACCAACTTG	Cloning of NCU01380 ^{JW228} in pMF272
80JW228_REco RI	ACAgaattcGTAGCTTTGGAGATCCTA	Cloning of NCU01380 ^{JW228} in pMF272

81JW228_FXbaI	ATAtctagaATGGCTGCCACAAGCAA	Cloning of NCU01381 ^{JW228} in pMF272
81JW228_REco RI	ATAgaattcCATTCCCTTTGCAAGGC	Cloning of NCU01381 ^{JW228} in pMF272
82JW228_FXbaI	ATAtctagaATGGGCGTGGGAAAGTTCT	Cloning of NCU01382 ^{JW228} in pMF272
82JW228_RPsp OMI	AAAgggcccTTTTATACCGAGAAAGTACA	Cloning of NCU01382 ^{JW228} in pMF272
cwr-1_wt_F	ATAgeggeegeACTGATTCATGCGGTAAA	Cloning of wild type <i>cwr-1</i> in pMF272
cwr-1_wt_R	CGCgaattcCTTTTTCAGGGCCACCATC	Cloning of wild type NCU01380 in pMF272
cwr-1_Y159A_F	CCGAGAGTTCGCTATGAACTGTG	Site-directed mutagenesis of NCU01380
cwr- 1_Y159A_R	CACAGTTCATAGCGAACTCTCGG	Site-directed mutagenesis of NCU01380
cwr- 1_JW228_insert FW	ggtgtacagcatgcgctagcATGCACTTCACCAACTT GAT	Cloning of NCU01380 ^{JW228} in pCSR-1
cwr- 1_JW228_vector RV	ATCAAGTTGGTGAAGTGCATgctagcgcatgctgt acacc	Cloning of NCU01380 ^{JW228} in pCSR-1
cwr- 1_D111_insertF W	ggtgtacagcatgcgctagcATGTTCTTCACACAAG CTTT	Cloning of NCU01380 ^{D111} in pCSR-1
cwr- 1_D111_vectorR V	AAAGCTTGTGTGAAGAACATgctagcgcatgctg tacacc	Cloning of NCU01380 ^{D111} in pCSR-1
cwr- 1_JW228_D111 _vectorFW	ccgttcgtttcaggggttaattaattaatttaatagctccatgtcaacaa g	Cloning of NCU01380 ^{JW228} and NCU01380 ^{D111} in pCSR-1
cwr- 1_JW228_D111 _insertRV	ggagctattaaattaattaacccctgaaacgaacgg	Cloning of NCU01380 ^{JW228} and NCU01380 ^{D111} in pCSR-1

^{*,} for the generation of the Δ NCU01380 Δ NCU01382 double mutant, a PCR construct to delete NCU01382 was obtained (containing a nourseothricin resistance cassette) by PCR and transformed into a Δ NCU01380 strain (expressing a hygromycin B resistance cassette).

Table S2. Primers used in this study. Related to Figures 3-5

Abbre viation	Species	f. sp.	Strain name	NCU01379 ortholog	NCU01380 ortholog	NCU01381 ortholog	NCU01382 ortholog	
Nc	Neurospora crassa	-	FGSC2489	XP_960936	XP_960937	XP_960938	XP_960939	
Nc	Neurospora crassa	-	JW258					
Nc	Neurospora crassa	-	JW196					
Nc	Neurospora crassa	-	JW242					
Nc	Neurospora crassa	-	JW199					
Nc	Neurospora crassa	-	JW228					
Nc	Neurospora crassa	-	D111					
Nd	Neurospora discreta	-	AKFA16					
Nd	Neurospora discreta	-	AKFA10		[S1, S	3]		
Nd	Neurospora discreta	-	AKFA31					
Nd	Neurospora discreta	-	AKFA6					
Nd	Neurospora discreta	-	AKFA24					
Nd	Neurospora discreta	-	AKFA12					
Nd	Neurospora discreta	-	AKFA2					
Nd	Neurospora discreta	-	CAMH1105					
Nd	Neurospora discreta	-	AKFA20					
Nd	Neurospora discreta	-	FGSC8579	Neudi1 71353	Neudi1 164991	Neudi1 164992	Neudi1 123145	
Nt	Neurospora tetrasperma	-	FGSC2508	XP_009847286	XP_00984792 8	XP_0098479 27	XP_00984792 6	
Nt	Neurospora tetrasperma	-	FGSC2509	EGZ75311	EGZ75312	EGZ75313	EGZ75314	
Nt	Neurospora tetrasperma	-	СЈ01					
Nt	Neurospora tetrasperma	-	СЈ02					
Nt	Neurospora tetrasperma	-	СЈ03		[CO C	01		
Nt	Neurospora tetrasperma	-	СЈ04		[S8, S	9]		
Nt	Neurospora tetrasperma	-	CJ05					
Nt	Neurospora tetrasperma	_	СЈ07					

	1	1		1			
Nt	Neurospora tetrasperma	-	CJ08				
Nt	Neurospora tetrasperma	-	CJ73				
Nt	Neurospora tetrasperma	-	CJ85				
Nt	Neurospora tetrasperma	-	965a				
Fg	Fusarium graminearum	-	PH-1	XP_011324713	XP_01132471	XP_0113247 12	XP_01132471 0
Fg	Fusarium graminearum	-	CS3005	EYB33121	EYB33119	EYB33120	EYB33470
Fg	Fusarium graminearum	-	ITEM124	PCD19322	PCD19324	PCD19323	PCD19325
Fps	Fusarium pseudo- graminearum	-	CS3096	XP_009255638	XP_00925563	XP_0092556 36	XP_00925563 5
Fo	Fusarium oxysporum	-	FOSC3-a	EWZ02246	EWZ02249	EWZ02247, EWZ02248	EWZ02250
Fo	Fusarium oxysporum	-	Fo47	EWZ48329	EWZ48332	EWZ48330, EWZ48331	EWZ48333
Foce	Fusarium oxysporum	f. sp. cepae	A28	RKL04166	RKL04196	RKL04185	RKL04184
Foce	Fusarium oxysporum	f. sp. cepae	СВЗ	RKL09064	RKL09062	RKL09063	RKL09061
Foce	Fusarium oxysporum	f. sp. cepae	A13	RKK69029	RKK69027	RKK69028	RKK69046
Fo	Fusarium oxysporum	-	V64-1	SCO82169	SCO82171	SCO82170	SCO82172
Foce	Fusarum oxysporum	f. sp. cepae	Fus2	RKK24812	RKK24810	RKK24813	RKK24811
Foce	Fusarum oxysporum	f. sp. cepae	125	RKK62586	RKK62600	RKK62634	RKK62599
For	Fusarium oxysporum	f. sp. raphani	54005	EXK97096	EXK97091	EXK97094	EXK97090
Fol	Fusarium oxysporum	f. sp. lycopersici	4287	XP_018243601	XP_01824359 6	XP_0182435 99	XP_01824359 5
Fol	Fusarium oxysporum	f. sp. lycopersici	MN25	EWZ93401	EWZ93405	EWZ93403	EWZ93406
Fop	Fusarium oxysporum	f. sp. pisi	HDV247	EXA42116	EXA42111	EXA42114	EXA42110
Fop	Fusarium oxysporum	f. sp. pisi	T415	FusoxT415 64391 4	FusoxT415 21 3834	FusoxT415 2 13802	FusoxT415 21 3849
Fon	Fusarium oxysporum	f. sp. narcissi	N139	RYC94909	RYC94911	RYC94964	RYC94910
Foco	Fusarium oxysporum	f. sp. conglutinans	race2	EXL80329	EXL80334	EXL80332	EXL80335
Fov	Fusarium oxysporum	f. sp. vasinfectum	25433	EXM33843	EXM33847	EXM33845	EXM33848
Fo	Fusarium oxysporum	-	5176	EGU85467	EGU85465	EGU85466	EGU85464
Forl	Fusarium oxysporum	f. sp. radicis- lycopersici	26381	EXL53658	EXL53662	EXL53661	EXL53663
Forc	Fusarium oxysporum	f. sp.radicis- cucumerinum	016	PCD41561	PCD41559	PCD41560	PCD41558
	. , ,						

Ft	Fusarium tricinctum	-	MPI-SDFR- AT-0044	Fustri1 488323	Fustri1 34050 5	Fustri1 64700 8	Fustri1 48925
Ft	Fusarium tricinctum	-	MPI-SDFR- AT-0068	Fustr1 191053	Fustr1 191034	Fustr1 54531	Fustr1 528039
Ff	Fusarium fujikuroi	-	IMI58289	XP_023429181	XP_02342918 0	XP_0234296 01	XP_02342917 9
Ff	Fusarium fujikuroi	-	C1995	SCN91243	SCN91247	SCN91245	SCN91248
Ff	Fusarium fujikuroi	-	B14	SCV54708	SCV54704	SCV54705	SCV54703
Ff	Fusarium fujikuroi	-	FSU48	SCV34075	SCV34077	SCV34076	SCV34078
Ff	Fusarium fujikuroi	-	NCIM1100	SCO37804	SCO37801	SCO37803	SCO37800
Ff	Fusarium fujikuroi	-	E282	SCO01987	SCO01995	SCO01993	SCO01997
Ff	Fusarium fujikuroi	-	B20	SCN74057	SCN74067	SCN74061	SCN74070
Ff	Fusarium fujikuroi	-	m567	SCN95983	SCN95976	SCN95978	SCN95973
Ff	Fusarium fujikuroi	-	MRC2276	SCO40913	SCO40907	SCO40908	SCO40905
Ff	Fusarium fujikuroi	-	KSU3368	KLO91625	KLO91627	KLO91626	KLO91628
Fpr	Fusarium proliferatum	-	NRRL6290 5	CVK88004	CVK88002	CVK88003	CVK88001
Fpr	Fusarium proliferatum	-	ITEM 2341	RBA08679	RBA08681	RBA08680	RBA08682
Fpr	Fusarium proliferatum	-	A8	RKL41765	RKL41763	RKL41766	RKL41764
Fpr	Fusarium proliferatum	-	ET1	CZR38825	CZR38827	CZR38826	CZR38828
Fv	Fusarium verticillioides	-	BRIP53590	RBR10139	RBR10137	RBR10138	RBR10163
Fv	Fusarium verticillioides	-	BRIP53263	RBQ90282	RBQ90280	RBQ90281	RBQ90288
Fv	Fusarium verticillioides	-	BRIP14953	RBQ75871	RBQ75869	RBQ75870	RBQ75879
Fv	Fusarium verticillioides	-	7600	XP_018749309	XP_01874930 5	XP_0187493 06	XP_01874930 4
-	Trichoderma harzianum	-	Т6776	KKP04788	KKP04790	KKP04789	KKP04791
-	Trichoderma harzianum	-	TR274	PKK52483	PKK52487	PKK52502	PKK52488
-	Trichoderma harzianum	-	CBS226.95	XP_024777899	XP_02477790 3	XP_0247779 00	XP_02477790 4
-	Trichoderma harzianum	-	M10	TriharM10_1 479 745	TriharM10_1 256810	TriharM10_1 422315	TriharM10_1 371291
-	Trichoderma harzianum	-	T22	TriharT22_1 3131 79	TriharT22_1 3 13041		TriharT22_1 4 61556
-	Zymoseptoria tritici	-	IPO323	XP_003850475	XP_00385003 0	XP_0038503	XP_00385039 2
-	Zymoseptoria tritici	-	ST99CH_3 D7	SMQ53153	SMQ53351	SMQ53397	SMQ53352

	Zymoseptoria	_	ST99CH_1	SMY26785	SMY26981	SMY27029	SMY26982
	tritici		A5				
	Zymoseptoria		ST99CH_3	SMR59590	SMR59792	SMR59840	SMR59793
_	tritici	-	D1 _				
	Zymoseptoria		ST99CH_1	SMR56737	SMR56932	SMR56979	SMR56933
-	tritici	-	E4 _				

Table S3. Abbreviations and accession numbers. Related to Figures 6 and S6.

Supplemental References

- S1. Heller, J., Zhao, J., Rosenfield, G., Kowbel, D.J., Gladieux, P., and Glass, N.L. (2016). Characterization of greenbeard genes involved in long-distance kind discrimination in a microbial eukaryote. PLoS Biol. *14*, e1002431.
- S2. Otsu, N. (1979). Threshold selection method from gray-level histograms. IEEE T. Syst. Man. Cyb. *9*, 62-66.
- S3. Heller, J., Clave, C., Gladieux, P., Saupe, S.J., and Glass, N.L. (2018). NLR surveillance of essential SEC-9 SNARE proteins induces programmed cell death upon allorecognition in filamentous fungi. Proc. Natl. Acad. Sci. U. S. A. *115*, E2292-E2301.
- S4. Fleissner, A., Leeder, A.C., Roca, M.G., Read, N.D., and Glass, N.L. (2009). Oscillatory recruitment of signaling proteins to cell tips promotes coordinated behavior during cell fusion. Proc. Natl. Acad. Sci. U. S. A. *106*, 19387-19392.
- S5. Freitag, M., and Selker, E.U. (2006). Expression and visualization of red fluorescent protein (RFP) in *Neurospora crassa*. Fungal Genet. Newsl. *52*, 14-17.
- S6. Ellison, C.E., Hall, C., Kowbel, D., Welch, J., Brem, R.B., Glass, N.L., and Taylor, J.W. (2011). Population genomics and local adaptation in wild isolates of a model microbial eukaryote. Proc. Natl. Acad. Sci. U. S. A. *108*, 2831-2836.
- S7. McCluskey, K., Wiest, A., and Plamann, M. (2010). The Fungal Genetics Stock Center: a repository for 50 years of fungal genetics research. J. Biosci. *35*, 119-126.
- S8. Corcoran, P., Anderson, J.L., Jacobson, D.J., Sun, Y., Ni, P., Lascoux, M., and Johannesson, H. (2016). Introgression maintains the genetic integrity of the mating-type determining chromosome of the fungus *Neurospora tetrasperma*. Genome Res. *26*, 486-498.
- S9. Sun, Y., Svedberg, J., Hiltunen, M., Corcoran, P., and Johannesson, H. (2017). Large-scale suppression of recombination predates genomic rearrangements in *Neurospora tetrasperma*. Nat. Commun. *8*, 1140.